Clinical Characteristics and Genetic Background of Congenital Long-QT Syndrome Diagnosed in Fetal, Neonatal, and Infantile Life

A Nationwide Questionnaire Survey in Japan

Hitoshi Horigome, MD; Masami Nagashima, MD; Naokata Sumitomo, MD; Masao Yoshinaga, MD; Hiroya Ushinohama, MD; Mari Iwamoto, MD; Junko Shiono, MD; Koh Ichihashi, MD; Satoshi Hasegawa, MD; Tadahiro Yoshikawa, MD; Tamotsu Matsunaga, MD; Hiroko Goto, MD; Kenji Waki, MD; Masaki Arima, MD; Hisashi Takasugi, MD; Yasuhiko Tanaka, MD; Nobuo Tauchi, MD; Masanobu Ikoma, MD; Noboru Inamura, MD; Hideto Takahashi, PhD; Wataru Shimizu, MD; Minoru Horie, MD

Background—Data on the clinical presentation and genotype-phenotype correlation of patients with congenital long-QT syndrome (LQTS) diagnosed at perinatal through infantile period are limited. A nationwide survey was conducted to characterize how LQTS detected during those periods is different from that in childhood or adolescence.

Methods and Results—Using questionnaires, 58 cases were registered from 33 institutions. Diagnosis (or suspicion) of LQTS was made during fetal life (n=18), the neonatal period (n=31, 18 of them at 0 to 2 days of life), and beyond the neonatal period (n=9). Clinical presentation of LQTS included sinus bradycardia (n=37), ventricular tachycardia/torsades de pointes (n=27), atrioventricular block (n=23), family history of LQTS (n=21), sudden cardiac death/aborted cardiac arrest (n=14), convulsion (n=5), syncope (n=5), and others. Genetic testing was available in 41 (71%) cases, and the genotype was confirmed in 29 (71%) cases, consisting of LQT1 (n=11), LQT2 (n=11), LQT3 (n=6), and LQT8 (n=1). Ventricular tachycardia/torsades de pointes and atrioventricular block were almost exclusively observed in patients with LQT2, LQT3, and LQT8, as well as in those with no known mutation. In LQT1 patients, clues to diagnosis were mostly sinus bradycardia or family history of LQTS. Sudden cardiac death/aborted cardiac arrest (n=14) was noted in 4 cases with no known mutations as well as in 4 genotyped cases, although the remaining 6 did not undergo genotyping. Their subsequent clinical course after aborted cardiac arrest was favorable with administration of β-blockers and mexiletine and with pacemaker implantation/implantable cardioverter-defibrillator.

Conclusions—Patients with LQTS who showed life-threatening arrhythmias at perinatal periods were mostly those with LQT2, LQT3, or no known mutations. Independent of the genotype, aggressive intervention resulted in effective suppression of arrhythmias, with only 7 deaths recorded. (***Circ Arrhythm Electrophysiol.* 2010;3:10-17.)**

Key Words: arrhythmia ■ long-QT syndrome ■ genes ■ death (sudden)

Congenital long-QT syndrome (LQTS) is an inherited disorder characterized by polymorphic ventricular tachycardia (VT), or torsades de pointes (TdP), syncope, and sudden cardiac death.[1] LQTS is often diagnosed in children from school age to young adulthood[2] and sometimes during fetal, neonatal, and infantile life.[3–5] Previous case reports

Received June 9, 2009; accepted November 19, 2009.

From the Department of Child Health (H.H.), Graduate School of Comprehensive Human Sciences, University of Tsukuba, Tsukuba, Japan; the Department of Cardiology (M.N.), Aichi Children's Health and Medical Center, Ohbu, Japan; the Department of Pediatrics and Child Health (N.S.), Nihon University School of Medicine, Tokyo, Japan; the Department of Pediatrics (M.Y.), National Hospital Organization Kagoshima Medical Center, Kagoshima, Japan; the Department of Cardiology (H.U.), Fukuoka Children's Hospital and Medical Center for Infectious Diseases, Fukuoka, Japan; the Department of Pediatric Cardiology (M. Iwamoto), Yokohama City University School of Medicine, Yokohama, Japan; the Department of Pediatrics (J.S.), Ibaraki Children's Hospital, Mito, Japan; the Department of Pediatrics (K.I.), Jichi Medical University, Shimotsuke, Japan; the Department of Pediatrics (S.H.), Niigata University Graduate School of Medical and Dental Science, Niigata, Japan; the Department of Pediatrics (T.Y.), Sakakibara Heart Institute, Fuchu, Japan; the Department of Pediatric Cardiology (T.M.), International Medical Center, Saitama Medical University, Hidaka, Japan; the Department of Pediatrics (H.G.), Gifu Prefectural General Medical Center, Gifu, Japan; the Department of Pediatrics (K.W.), Kurashiki Central Hospital, Kurashiki, Japan; the Department of Pediatrics (M.A.), Sent Marianna University School of Medicine, Kawasaki, Japan; the Department of Pediatrics (H. Takasugi), Kochi Medical School, Kochi, Japan; the Department of Cardiology (Y.T.), Shizuoka Children's Hospital, Shizuoka, Japan; the Department of Pediatric Cardiology (N.T.), Ogaki Municipal Hospital, Ogaki, Japan; the Department of Pediatrics (M. Ikoma), Japanese Red Cross Nagoya Daiichi Hospital, Nagoya, Japan; the Department of Pediatric Cardiology (N.I.), Osaka Medical Center and Research Institute for Maternal and Child Health, Izumi, Japan; the Department of Epidemiology and Biostatistics (H. Takahashi), School of Medicine, University of Tsukuba, Tsukuba, Japan; the Division of Cardiology (W.S.), Department of Internal Medicine, National Cardiovascular Center, Suita, Japan; and the Department of Cardiology and Respiratory Medicine (M.H.), Shiga University of Medical Science, Otsu, Japan.

Correspondence to Hitoshi Horigome, MD, PhD, Department of Child Health, Graduate School of Comprehensive Human Sciences, University of Tsukuba, 1-1-1 Tennodai, Tsukuba 305-8575, Japan. E-mail hhorigom@md.tsukuba.ac.jp

Circ Arrhythm Electrophysiol **is available at http://circep.ahajournals.org** **DOI: 10.1161/CIRCEP.109.882159**

Table 1. Questionnaire Items

1. Patient: Serial No. in each institution, initials, birth year, and month, sex
2. Age at diagnosis or suspicion (including gestational age for a fetus)
3. Clinical symptoms: Fetal arrhythmias, fetal heart failure, syncope, convulsion, heart failure, aborted cardiac arrest, others
4. ECG findings and arrhythmias (heart rate, QTc on ECG at presentation, sinus bradycardia, VT/TdP, atrioventricular block, other arrhythmias)
5. Family history of LQTS or other arrhythmias or sudden cardiac death (which member, and their outcome?)
6. Genotype
7. Treatment (acute therapy and maintenance therapy)
   pharmacotherapy (which drug, dose, age at initiation, and duration)
   device therapy (pacemaker implantation/implantable cardioverter-defibrillator) and age at application
8. Duration of follow-up
9. Outcome (alive or death, and neurological sequels of cardiac arrest)

suggest that the latter cases are at higher risk of development of life-threatening arrhythmias necessitating emergency treatment[3–5] and show higher mortality rates than the former age groups.[3,5–11] For example, recent progress in molecular biology has clarified that LQTS partly contributes to sudden infant death syndrome (SIDS).[12,13] Unfortunately, prenatal diagnosis of LQTS has been extremely difficult to confirm except for a limited number of cases for which prenatal gene screening[14] or fetal magnetocardiography (fMCG)[15–17] was applied.

Clinical Perspective on p 17

Thus, the clinical presentation, the genotype-phenotype correlation, and the outcome of patients with fetal, neonatal, or infantile presentation of LQTS remain to be elucidated. The purposes of this study were first, to report the findings of a nationwide survey conducted to define the clinical characteristics and the genotype-phenotype correlation, and second, to report the outcome of patients with LQTS diagnosed before birth and in the first year of life.

Methods

Population

The study population included fetuses, neonates, and infants (<1 year of age) diagnosed with LQTS based on ECG findings including prolonged QTc >0.46 seconds (using Bazett formula), with or without VT/TdP, who had no structural heart disease, family history of LQTS, or had undergone genetic testing. Those with normal QTc duration and no gene mutation known to cause LQTS were excluded. Patient data were collected using questionnaires. The form was sent to those councilors of the Japanese Society of Pediatric Cardiology and Cardiac Surgery who responded to a preliminary survey that they had 1 or more cases of LQTS diagnosed during fetal, neonatal, and infantile life. The items obtained from the responders are presented in Table 1.

The study protocol was approved by the Ethics Committee of the University Hospital of Tsukuba, and informed consent was obtained from each patient (or parents, if the patient was younger than 15 years of age) by a coordinator in charge in each institution before the patient's data were registered.

Genetic Analysis and Genotype-Phenotype Correlation

Genetic analyses were performed in 4 established laboratories in Japan. DNA was isolated from blood samples in each patient. Screening for mutations of at least 3 major genes causing LQTS (*KCNQ1, KCNH2, SCN5A*) was performed using polymerase chain reaction (PCR)/single-strand conformation polymorphism or denatured high-performance liquid chromatography analysis. For aberrant PCR products, DNA sequencing was conducted with a DNA sequencer (ABI 3700 and ABI 3130xl, Applied Biosystems, Foster City, Calif). For those subjects in whom genotype was confirmed and those who underwent genetic analysis but found to have no mutation, genotype-phenotype correlations (or mutation-negative phenotype correlations) with the aforementioned items (Table 1) were investigated.

Statistical Analysis

All statistical calculations were conducted using the R software. Quantitative variables (heart rate [HR] and QTc) are presented as mean±SD and categorized variables (presence of FH, sinus bradycardia, VT/TdP, and atrioventricular block [AVB]) as proportions (percentages). One-way ANOVA was applied for comparisons of continuous variables, followed by pairwise comparisons with Bonferroni adjustment of probability values among 4 groups (LQT1, LQT2, LQT3, and mutation-negative groups). The equality of proportions for categorical variables among the 4 groups was examined by the χ^2 test (global test). When there was a significant difference in proportions, we performed pairwise comparisons between pairs of proportions with correction for multiple testing using Bonferroni inequality of probability values. Tests were 2-sided, and a probability value <0.05 was considered significant.

The authors had full access to the data and take responsibility for its integrity. All authors have read and agreed to the manuscript as written.

Results

Population

A total of 58 cases (all Japanese; males 30, females 28) were registered from 33 institutions. Forty-one were born during the last 10 years (between 1999 and 2008), 14 between 1989 and 1998, 1 in 1986, and 2 in 1984. LQTS was diagnosed or suspected during fetal life at 18 to 40 weeks of gestation in 18 individuals, during neonatal life at 0 to 28 days in 31, and in infancy (<1 year) at 1 to 9 months in 9.

Clinical Features

For 18 fetuses with LQTS, clinical presentation (or clues to diagnosis or suspicion of LQTS) included bradycardia (15 cases), AVB (8 cases), VT/TdP (7 cases), and family history of LQTS (6 cases), including 1 family with a previous intrauterine death (items overlapped in some cases). Two fetuses were confirmed to be LQTS by fMCG, with QTc values of 570 and 680 on fMCG, and 590 and 700 on ECG soon after birth, respectively (these 2 cases have been reported previously).[16,17] No fetal death was noted in this group.

For 31 neonates with LQTS, the most frequent feature was sinus bradycardia (17 cases), followed by VT/TdP (15 cases), positive family history of LQTS (15 cases), including 1 with previous intrauterine death and 1 with infantile death, AVB (10 cases), syncope (5 cases), convulsion (5 cases), and others (items overlapped in some cases). Among the 31 neonatal cases, 18 (70%) were diagnosed within 2 days of life, and 8 of them had some significant fetal presentation (4 bradycardia or bradyarrhythmias, 4 tachyarrhythmias, and 1 hydrops), retrospectively.

As described above, the number of patients with LQTS diagnosed during infancy beyond the neonatal period was only 9. The clinical presentation of these patients included sinus bradycardia (5 cases), sudden cardiac death (SCD)/

aborted cardiac arrest (ACA) (5 cases), AVB (5 cases), VT/TdP (5 cases), and other miscellaneous abnormalities.

The ECG on diagnosis, or immediately after birth for fetal cases, showed that the HR and QTc interval (corrected using Bazett formula) ranged from 50 to 160 (102±28) bpm, and from 360 to 774 (563±70) ms, respectively.

Genotype-Phenotype Correlation

Among 41 patients who underwent genetic testing, mutations were identified in 29 (71%) cases; including *KCNQ1* gene mutations (LQT1) in 11, *KCNH2* mutations (LQT2) in 11, *SCN5A* mutations (LQT3) in 6, and *CACNA1C* (LQT8) in 1. Twelve patients also underwent genotyping, but no mutation was found. Table 2 lists the demographic and clinical features of these subjects (references 16, 17, and 23 reported the same cases 2, 12, and 27 in Table 2) and of those with no known mutations.

The remaining 17 subjects (6 fetuses, 8 neonates, 3 infants) did not undergo genetic analysis due to lack of such analysis at that time, death soon after birth, or refusal by parents. Five had SCD/ACA (Table 3), including a 1-day-old neonate who had AVB and died at 57 days of age in 1984. This case was later assumed to be LQT8, based on characteristic phenotypes such as syndactyly. AVB and VT/TdP were observed in 7 and 5 cases, respectively, in this group.

Although HR and QTc values were not different among LQT1, LQT2, LQT3, and mutation-negative groups, the incidence of VT/TdP was higher in LQT2 and LQT3 compared with LQT1 (Table 4). The incidence of AVB tended to be higher in LQT3 compared with LQT1 but statistically insignificant. On the other hand, the presence of family history of LQTS was more frequent in LQT1 than the mutation-negative group. The incidence of sinus bradycardia was comparable among the 4 groups (Table 4).

Table 3 lists cases with SCD/ACA; only 4 genetically confirmed cases were included, and 4 were mutation-negative, although the remaining 6 cases did not undergo genotyping. These individuals showed bradycardia (97±31 bpm; 10/14 showed HR <110 bpm) and markedly prolonged QTc (617±81 ms).

Treatment

With regard to the treatment of fetal VT/TdP, antiarrhythmic agents were administered transplacentally in 4 of 18 fetal cases (propranolol in 3 cases, lidocaine in 1, mexiletine in 1, flecainide in 1, and magnesium in 1), using the method described in detail in our previous report.[17] None of the 4 cases was genetically confirmed prenatally. When 2 or 3 of the following findings of sinus bradycardia, VT, and AVB were observed in a structurally normal heart, LQTS was strongly suggested, and β-blockers, sodium channel blockers (lidocaine, mexiletine), and magnesium (Mg) were selected as typical antiarrhythmic agents, instead of amiodarone or sotalol, which may prolong the QT interval. These drugs were used in combination until VT/TdP was controlled and proved effective in all 4 cases. However, preterm delivery was conducted in 2 cases both at 33 weeks of gestation due to recurrent VT/TdP and depression of fetal physical activity in one and to fetal hydrops and distress in the other. In the remaining 14 cases, pharmacotherapy was initiated after confirmation of the type of arrhythmias after birth. However, no fetal death was noted.

For 15 neonatal cases who presented with VT/TdP (including those who did not undergo genotyping), acute pharmacotherapy consisted of 2 or more of the following drugs: β-blockers, mexiletine, lidocaine, Mg, phenytoin, and others, except for 2 cases who were treated with phenytoin alone and 1 with mexiletine alone. Most of these cases were judged to respond the combination therapy. In 5 neonates in whom LQT3 was strongly suggested based on a typical ECG finding called late-appearing T wave, mexiletine was first administered but proved insufficient, and β-blockers were also added in all 5.

For those with LQTS presenting in infancy, 6 cases received acute pharmacotherapy (2 or all of propranolol, mexiletine, and Mg). No additional agent was administered. Thus, in all age groups, the acute therapy for VT/TdP consisted of a single drug to which 1 or more drugs was then added until the arrhythmia was controlled, independent of the genotype. Actually, the genotype was not identified during the acute phase in most cases. Furthermore, genotyping was not conducted in those 17 cases who presented before 1999.

Maintenance therapy consisted mainly of β-blockers (or no therapy) for LQT1 and mostly of mexiletine/β-blockers for LQT2 and LQT3 (Table 2). β-Blockers were added in 8 LQT2 cases after confirmation of the genotype. In all 6 LQT3 cases, mexiletine was maintained (combined with β-blockers) from acute through chronic phase after determination of the genotype.

Nine patients underwent pacemaker implantation (PMI), 5 with ventricular pacing mode (VVI) and 1 with atrial pacing mode (AAI), from age 1 day to 8 years due to severe bradycardia caused by AVB, inducing VT/TdP. In 6 cases, VT was completely suppressed after PMI. Only 2 patients had an implantable cardioverter-defibrillator (ICD) at ages 4 (LQT3) and 25 months (mutation negative), respectively, due to recurrent VT/TdP with satisfactory results.

Outcome

During the follow-up period of 8 days to 23.5 years (median, 4.25 years), 7 SCD and 7 ACA were registered (age at SCD or ACA range, 8 days to 10 years; median, 10.5 months); 6 did not have genetic testing, whereas 4 showed no mutation. Only 4 were genetically confirmed (Table 3). One case was later suspected to be LQT8, based on the phenotype including syndactyly. Among the 14 SCD/ACA cases, 12 had been under pharmacotherapy, 5 with both β-blockers and sodium channel blockers, and 2 had had PM or ICD. Four cases developed significant neurological deficits after cardiorespiratory resuscitation.

Discussion

The noteworthy finding of the present study was that 49 of 58 cases (84%) were diagnosed at the fetal or neonatal period, although this survey covered the entire infantile period. Remarkably, two thirds of the neonatal cases were diagnosed within 2 days of life; this period should be recognized as the most vulnerable period. The number of cases diagnosed after the neonatal period was only 9. Considering that the average age at appearance of symptoms in LQT2 and LQT3 is after

Table 2. Clinicogenetic Details

Case	LQT Type	Mutation	Age at Diagnosis/Sex	Clinical Presentation	FH	HR, bpm	QTc, ms
1	LQT1	Thr587Met	Fetus/M	FH, brady	+	109	561
2	LQT1	Ala341Val	Fetus/M	Brady	+	110	590
3	LQT1	Ala341Val	Neonate/M	FH	+	110	520
4	LQT1	Ile313Lys	Neonate/M	FH	+	102	589
5	LQT1	Ile313Lys	Neonate/M	FH	+	115	554
6	LQT1	276delSer	Neonate/M	Prolonged QT	+	115	570
7	LQT1	Asp611Tyr	Neonate/M	Brady	+	80	550
8	LQT1	Asp611Tyr	Neonate/F	FH	+	ND	ND
9	LQT1	Thr458Met	Neonate/M	FH	+	126	530
10	LQT1	Gly643Ser	Infant/M	ACA	−	109	554
11	LQT1	Gly269Ser	Infant/F	Cyanosis	−	113	586
					82%	109±12	560±24
12	LQT2	Gly628Ser	Fetus/M	VT/TdP, AVB	−	50	631
13	LQT2	del(7)(q32qter)	Fetus/F	TdP	−	111	492
14	LQT2	Ser243+112X	Fetus/F	FH	+	160	360
15	LQT2	Gly628Ala	Fetus/F	Syncope, VT/TdP, AVB	+	78	570
16	LQT2	Thr613Met	Fetus/M	VT/TdP, AVB	−	60	578
17	LQT2	Ala561Val	Neonate/M	Cyanosis, VT/TdP	−	86	520
18	LQT2	Gly628Ser	Neonate/M	TdP, brady	−	111	550
19	LQT2	Thr613Met	Neonate/M	convulsion, VT	−	140	599
20	LQT2	Gly572Ser	Neonate/F	TdP, AVB	−	91	520
21	LQT2	Ala614Val	Neonate/F	Syncope, VT	+	98	500
22	LQT2	Asn633Ser	Infant/F	VT/TdP, AVB	−	60	600
					27%	95±34	538±74
23	LQT3	Ala1186Thr	Fetus/M	AVB	+	78	679
24	LQT3	Asn1774Asp	Fetus/M	convulsion, VT/TdP, AVB	−	115	670
25	LQT3	Val176Met	Neonate/F	TdP, AVB	+	63	600
26	LQT3	Asn406Lys	Neonate/M	Syncope, TdP	+	129	598
27	LQT3	Arg1623Gln	Neonate/F	Heart failure	−	79	483
28	LQT3	Leu1772Val	Infant/M	ACA	−	138	520
					50%	100±31	592±79
29	LQT8	Gly406Arg	Neonate/M	AVB	−	141	581
30	Unidentified	−	Fetus/F	Brady	+	80	554
31	Unidentified	−	Fetus/M	Brady	−	100	510
32	Unidentified	−	Fetus/M	VT	−	85	590
33	Unidentified	−	Fetus/M	AVB	−	80	600
34	Unidentified	−	Neonate/F	Syncope	−	100	647
35	Unidentified	−	Neonate/F	Arrhythmia	−	126	586
36	Unidentified	−	Neonate/F	ACA	−	111	638
37	Unidentified	−	Neonate/M	Brady	−	93	550
38	Unidentified	−	Neonate/F	FH	+	120	520
39	Unidentified	−	Infant/F	ACA	−	160	470
40	Unidentified	−	Infant/F	ACA	−	100	774
41	Unidentified	−	Infant/F	PAC with block	−	60	460
					17%	104±32	575±86

(Continued)

Cases 2, 12, and 27 are reported in references 16, 17, and 23, respectively. ACA indicates aborted cardiac arrest; AVB, atrioventricular block; BB, β-blocker; brady, bradycardia; FH, family history; HR, heart rate; ICD, implantable cardioverter-defibrillator; Isp, isoproterenol; Lido, lidocaine; Mexil, mexiletine; Mg, magnesium; Nifed, nifedipine; PAC, premature atrial contraction; Pheny, phenytoin; PM, pacemaker; SCD, sudden cardiac death.

Table 2. Continued

Sinus Brady	VT/TdP	AVB	Acute Therapy	Maintenance Therapy	PMI/ICD	Follow-Up	Outcome
+	–	+	–	–	–	0 mo	Alive
+	–	–	–	BB	–	9 y	Alive
+	–	–	–	BB	–	4 y, 1 mo	Alive
+	–	–	–	BB	–	11 y, 10 mo	Alive
+	–	–	–	BB	–	10 mo	Alive
+	–	–	–	–	–	11 mo	Alive
+	–	–	–	–	–	7 y, 3 mo	Alive
+	–	–	–	–	–	5 y, 8 mo	Alive
–	–	–	–	–	–	4 y, 5 mo	Alive
+	–	–	Lido, Mexil	Mexil	–	9 y, 1 mo	Alive
+	–	–	–	–	–	7 y, 8 mo	Alive
73%	0%	9%				Median 68 mo	
+	+	+	Lido, Mg, BB, Mexil, Pacing	BB, Mexil	PM	3 y	Alive
+	+	–	–	BB	–	1 y	Alive
–	–	–	–	BB	–	2 y, 2 mo	Alive
+	+	+	Lido, Mg, BB, Mexil, pacing	BB, Mexil	PM	8 y, 1 mo	Alive
+	+	+	Mg, Mexil	BB, Mexil	–	8 mo	Alive
+	+	–	Lido, Mg, Mexil	BB, Mexil	–	11 y, 4 mo	Alive
+	+	+	Mexil	BB, Mexil	–	7 mo	Alive
–	+	–	Mg, BB	BB	–	8 y	Alive
+	+	+	Pheny	BB, Mexil	–	18 y, 5 mo	Alive
+	+	–	Pheny, DC	Pheny, BB	–	23 y, 6 mo	Alive
+	+	+	–	BB, Mexil	PM	15 y, 4 mo	Alive
82%	91%	55%				Median 96 mo	
+	+	+	Mexil	Mexil	PM ICD	3 y, 4 mo	Alive
+	+	+	BB, Mexil, Mg	BB, Mexil, Flecainide	PM	11 y, 4 mo	Alive
+	+	+	Lido, Mg, BB, Mexil	BB, Mexil	–	1 y, 3 mo	Alive
+	+	–	Lido, BB	BB, Mexil	–	11 mo	Alive
+	+	+	BB, Mexil, Lido	BB, Mexil	PM	8 y	Alive
–	+	+	Mg, BB, Mexil	BB, Mexil	–	3 y, 2 mo	Alive
83%	100%	83%				Median 39 mo	
–	+	+	BB, Mexil, Nifed	BB, Mexil, Nifed	–	3 y, 2 mo	Alive
+	–	+	–	BB, Mexil	–	2 y, 5 mo	Alive
+	–	–	–	BB	–	6 y, 5 mo	Alive
+	+	–	Lido, Mg	Mexil	–	5 y, 5 mo	Alive
+	–	+	BB, Mexil, Mg	BB, Mexil	–	4 mo	Alive
+	–	–	Lido, Mg, Isp	Mexil	–	4 y, 3 mo	Died
+	+	–	BB, Mg	BB	–	9 y, 5 m	Alive
–	+	–	Lido, BB, pheny, Mexil	Mexil	–	11 y, 9 mo	Alive
+	–	–	–	–	–	9 y, 6 mo	Alive
–	–	–	–	–	–	6 mo	Alive
–	+	–	BB, Mexil	BB, Mexil	ICD	7 y, 2 mo	Alive
+	+	+	Mexil	Mexil	–	4 y3 mo	Alive
+	–	–	BB, Mexil	BB, Mexil	–	7 y, 5 mo	Alive
75%	42%	25%				Median 71 mo	

Table 3. Clinicogenetic Details of Cases With Sudden Cardiac Death or Aborted Cardiac Arrest

Case	Case No. in Table 2	Genotyping	Age at Diagnosis	Age at SCD or ACA	HR, bpm	QTc, ms	Maintenance Therapy Until SCD/ACA	Acute Therapy for SCD/ACA Event
1	23	LQT3 (Ala1186Thr)	Fetus (28 wk)	1 y, 10 mo (aborted)	78	679	Mexil	Mexil, DC
2	...	No gene test	Fetus (31 wk)	8 d	60	570	...	Lido, Isp, Pacing, DC
3	...	No gene test	Fetus (36 wk)	57 d	90	600	BB, Mexil	DC
4	29	LQT8 (Gly406Arg)	Neonate (0 d)	1 y, 5 mo (aborted)	141	581	BB, Nifed	Mexil, Mg
5	...	Negative result	Neonate (0 d)	4 y	100	647	Mexil	DC
6	...	Negative result	Neonate (0 d)	<1 mo (aborted)	111	638	Mexil	Lido, Mexil, BB, Pheny
7	17	LQT2 (Ala561Val)	Neonate (1 d)	10 y (aborted)	86	520	BB, Mexil	Lido, Mexil, Mg, DC
8	...	No gene test (possible LQT8)*	Neonate (1 d)	57 d	70	640	BB	...
9	...	No gene test	Neonate (4 d)	5 y, 4 mo	60	590	... (refused)	...
10	...	No gene test	Infant (1 mo)	2 y	130	640	BB, Mexil	Lido, Mg
11	...	No gene test	Infant (1 mo)	1 y, 10 mo	60	740	BB, Mexil, PM	Lido, Mexil, BB, Mg, Pacing
12	10	LQT1 (Gly643Ser)	Infant (1 mo)	1 mo (aborted)	109	554	Mexil	Lido
13	39	Negative result	Infant (2 mo)	4 mo (aborted)	160	470	BB, Mexil, ICD	(aborted by ICD)
14	40	Negative result	Infant (2 mo)	2 mo (aborted)	100	774	Mexil	Mexil
				median 10.5 mo	97±31	617±81		

ACA indicates aborted cardiac arrest; BB, β-blocker; ICD, implantable cardioverter-defibrillator; Isp, isoproterenol; Lido, lidocaine; Mexil, mexiletine; Mg, magnesium; Nifed, nifedipine; Pheny, phenytoin; SCD, sudden cardiac death.

*LQT8 was retrospectively possible because phenotype included syndactyly.

school age,[2] we speculate a considerable number of patients are considered to go through infancy uneventfully.

Garson et al[4] reported 287 patients with LQTS age <21 years; their mean±SD age at presentation was 6.8±5.6; and 9% presented with cardiac arrest, 26% with syncope, and 10% with seizures. Although 20% of their subjects were <1 month of age, they did not investigate that age group separately. In the present study, confined to the subjects age <1, clinical features were largely different; that is, the incidence of malignant arrhythmias and bradycardia was high[6,7] whereas that of syncope and seizures was low.

Regarding genotype-phenotype correlations, Zareba et al[18] investigated child and adult LQTS and reported that LQT1 was associated with the highest risk of first cardiac event among the 3 most typical genotypes (LQT1–3). By the age of 15, syncope, ACA, or SCD was noted in 53% of their patients with LQT1 compared with 29% of LQT2 and 6% of LQT3, although cardiac events occurred in LQT3 were more lethal compared with those in LQT1 or LQT2. In contrast, the present study demonstrated that patients complicated by VT/TdP or AVB were almost exclusively those with LQT2 or LQT3 (and LQT8). LQT3 patients in the present study showed the most severe clinical course, similar to those in later-presenting LQT3. Further, patients with LQT1 mostly showed an uneventful clinical course apart from sinus bradycardia,[6] and the reason for diagnosis was bradycardia or prolonged QT interval itself on ECG identified on family screening. Another remarkable feature in our young age group was that a considerable number of patients with malignant arrhythmias were mutation-negative as far as LQT1–3 genes were typically examined. This suggests that this age group includes individuals with rare known mutations that were not examined in the present study as well as those with currently unidentifiable mutations.

Table 4. Comparison of Parameters Among the Groups

Parameter	LQT1 (n=11)	LQT2 (n=11)	LQT3 (n=6)	Negative (n=12)	Global Test	Pairwise Comparison
HR, bpm	109±12 (n=10*)	95±34	100±31	104±32	NS	
QTc, ms	560±24 (n=10*)	538±74	592±79	575±86	NS	
Proportion with family history, %	82	27	50	17	$P<0.05$	LQT1–Negative, $P<0.05$
Proportion with sinus bradycardia, %	73	82	83	75	NS	
Proportion with VT/TdP, %	0	91	100	42	$P<0.05$	LQT1–LQT2, $P<0.001$ LQT1–LQT3, $P<0.005$
Proportion with AVB, %	9	55	83	25	$P<0.05$	(LQT1–LQT3, $P=0.068$)

Data are mean±SD or %. One-way ANOVA was used to compare mean values of HR and QTc. χ^2 test was used to test differences in proportions of subjects with family history, sinus bradycardia, VT/TdP, and AVB among the 4 groups. Pairwise comparisons were conducted using Bonferroni adjustment and Bonferroni inequality of P value. NS indicates not significant; Negative, gene mutation-negative group.

*No. of cases is 10 because data were not available in 1 case.

Notably, many patients in the present study showed sinus bradycardia, although HR was not significantly different among LQT1, LQT2, and LQT3. Sinus bradycardia has been considered a significant presentation of LQTS, especially in the fetal-neonatal period,[3,19,20] and is often a clue to the diagnosis of LQTS. The present study verified that sinus bradycardia is common among all types of LQTS in this age group, especially in fetal-neonatal periods.

Another remarkable feature of the present study was the high incidence of AVB (55% in LQT2, 83% in LQT3), compared with 5% or less in child or adult LQTS.[4,20] It is intriguing that mutations in our LQT2 patients were almost exclusively located at the pore region of HERG gene (amino acid residues 550 through 650),[21] as mutations in that region are related to high risk for cardiac events.[21,22] Lupoglazoff et al[6] reported similar phenotype tendency for neonates with LQTS, that AVB is associated with LQT2 and sinus bradycardia with LQT1. Most of their LQT2 cases also had a mutation in the pore region of the HERG gene, although this was not mentioned in their report. AVB in neonates with an SCN5A mutation have also been reported in single case reports.[8,11,23,24] Considering the implication of sodium channel dysfunction in many other hereditary arrhythmias,[25] the association between LQT3 and AVB is an important finding.

SCD/ACA was seen in 14 cases (24% of all subjects) (7 SCD, 7 ACA), even though 12 of them were under treatment with β-blockers, mexiletine, or both when the events occurred (Table 3). The direct trigger of SCD/ACA remains to be determined, but the mean QTc interval of those patients was apparently prolonged (617±81 ms), and patients with no gene test (6 cases) were included as well, possibly making the selection of drugs inappropriate, such that only β-blockers were given to a possible LQT3 patient. Furthermore, 4 other cases had no known mutation on genotyping. It is possible that the cryptogenic mutations unidentifiable in the current era could be resistant to many drugs.

Therapy

Because individuals with LQT3 showed serious clinical disorders, they were treated aggressively with multiple antiarrhythmic drugs including mexiletine, β-blockers, lidocaine, Mg, and PM/ICD, and only 1 definite LQT3 patient showed ACA. For LQT2, malignant arrhythmias were a little more controllable with the same kind of pharmacotherapy than for LQT3. Again, only 1 definite LQT2 patient showed ACA. Thus, no death was ultimately observed in LQT2 and LQT3. This favorable clinical course might be derived from implicit strategy prevalent among pediatric cardiologists in our country that early-onset LQTS should be treated with the combination of β-blockers and mexiletine at the start of therapy because the genotype is not easy to confirm immediately. In other words, treatment strategies in Japan have been driven more by the clinical symptoms than by the genotype. Nevertheless, the response to the multiple antiarrhythmic pharmacotherapy and the long-term outcome presented in this study are encouraging.

It should be noted that the number of patients who underwent PMI/ICD was small in the present cohort compared with other reports.[5,6] It is known that TdP tends to follow a prolonged R-R interval in LQT2 and LQT3, in which conduction disturbances or sinus node dysfunction are common features.[25,26] Thus, PMI/ICD should be considered without delay even when the patient who shows drug-resistant, bradycardia-induced VT/TdP is a small baby.[27]

Study Limitations

Because of the retrospective nature of the present survey using questionnaires, the extent of clinical data that could be obtained varied among cases. Although approximate tendency in genotype-phenotype correlations for infants with LQT1, LQT2, and LQT3 was determined, most cases registered in the present study did not undergo genetic analysis for genes other than the 3 typical types. One case with LQT8 was registered in addition to LQT1–3, but no cases with the other types (LQT4–7) were found. Also, decision of treatment strategy depended on the in-charge physician in each case without the use of a uniform protocol for VT/TdP and/or AVB, making it difficult to evaluate the effects of pharmacotherapy and to determine the event rate beyond infancy for each genotype other than the last outcome, alive or death. Therefore, we should wait for accumulation of more cases for establishment of the genotype-specific strategy.

Conclusion

Our nationwide survey indicates that early-onset malignant LQTS are mostly those with LQT2 and LQT3 among the 3 major genes, and the most vulnerable age to life-threatening arrhythmias is from 0 to 2 days of age. A combination pharmacotherapy with a β-blocker and mexiletine sometimes combined with Mg and PMI/ICD is recommended as the initial therapy. Prospective study of a large number of patients with LQTS diagnosed from fetal to infantile periods and further application of gene testing are needed to establish the most appropriate treatment strategies for those patients.

Acknowledgments

We are grateful to Dr Minako Hoshiai, University of Yamanashi; Dr Fukiko Ichida, University of Toyama; Dr Hiroki Kajino, Asahikawa Medical College; Dr Masaru Miura, Tokyo Metropolitan Kiyose Children's Hospital; Dr Tomoaki Murakami, Hokkaido University; Dr Kiyoshi Ogawa, Saitama Children's Medical Center; Dr Hirofumi Saiki, Hyogo Children's Hospital; Dr Jun-ichi Sato, Funabashi Municipal Medical Center; Dr Hiroshi Shimizu, Chugoku Rosai Hospital; Dr Kenji Suda, Kurume University School of Medicine; Dr Hiroshi Suzuki, Yamagata University School of Medicine; Dr Jun-ichi Takagi, University of Miyazaki; Dr Sho Takeda, Seirei Hamamatsu General Hospital; Dr Kiyohiro Takigiku, Nagano Children's Hospital; and Dr Hiroyuki Yamagishi, Keio University, for their contribution to the survey.

Disclosures

Drs Shimizu and Horie were supported by the Health Sciences Research Grants (H18–Research on Human Genome–002) and a Research Grant for Cardiovascular Diseases (21C-8) from the Ministry of Health, Labor, and Welfare of Japan. The other authors declare no conflicts of interest.

References

1. Moss AJ, Kass RS. Long QT syndrome: from channels to cardiac arrhythmias. *J Clin Invest*. 2005;115:2018–2024.
2. Priori SG, Napolitano C, Schwartz PJ, Grillo M, Bloise R, Ronchetti E, Moncalvo C, Tulipani C, Veia A, Bottelli G, Nastoli J. Association of

long QT syndrome loci and cardiac events among patients treated with beta-blockers. *JAMA*. 2004;292:1341–1344.
3. Hofbeck M, Ulmer H, Beinder E, Sieber E, Singer H. Prenatal findings in patients with prolonged QT interval in the neonatal period. *Heart*. 1997; 77:198–204.
4. Garson A Jr, Dick M II, Fournier A, Gillette PC, Hamilton R, Kugler JD, van Hare GF III, Vetter V, Vick GW III. The long QT syndrome in children: an international study of 287 patients. *Circulation*. 1993;87: 1866–1872.
5. Gorgels AP, Al Fadley F, Zaman L, Kantoch MJ, Al Halees Z. The long QT syndrome with impaired atrioventricular conduction: a malignant variant in infants. *J Cardiovasc Electrophysiol*. 1998;9:1225–1232.
6. Lupoglazoff JM, Denjoy I, Villain E, Fressart V, Simon F, Bozio A, Berthet M, Benammar N, Hainque B, Guicheney P. Long QT syndrome in neonates: conduction disorders associated with HERG mutations and sinus bradycardia with KCNQ1 mutations. *J Am Coll Cardiol*. 2004;43: 826–830.
7. Shim SH, Ito M, Maher T, Milunsky A. Gene sequencing in neonates and infants with the long QT syndrome. *Genet Test*. 2005;9:281–284.
8. Chang CC, Acharfi S, Wu MH, Chiang FT, Wang JK, Sung TC, Chahine M. A novel SCN5A mutation manifests as a malignant form of long QT syndrome with perinatal onset of tachycardia/bradycardia. *Cardiovasc Res*. 2004;64:268–278.
9. Johnson WH, Yang P, Yang T, Lau YR, Mostella BA, Wolff DJ, Roden DM, Benson DW. Clinical, genetic, and biophysical characterization of a homozygous HERG mutation causing severe neonatal long QT syndrome. *Pediatr Res*. 2003;53:744–748.
10. Hoorntje T, Alders M, van Tintelen P, van der Lip K, Sreeram N, van der Wal A, Mannens M, Wilde A. Homozygous premature truncation of the HERG protein: the human HERG knockout. *Circulation*. 1999;100: 1264–1267.
11. Schulze-Bahr E, Fenge H, Etzrodt D, Haverkamp W, Monnig G, Wedekind H, Breithardt G, Kehl HG. Long QT syndrome and life threatening arrhythmia in a newborn: molecular diagnosis and treatment response. *Heart*. 2004;90:13–16.
12. Arnestad M, Crotti L, Rognum TO, Insolia R, Pedrazzini M, Ferrandi C, Vege A, Wang DW, Rhodes TE, George AL Jr, Schwartz PJ. Prevalence of long-QT syndrome gene variants in sudden infant death syndrome. *Circulation*. 2007;115:361–367.
13. Otagiri T, Kijima K, Osawa M, Ishii K, Makita N, Matoba R, Umetsu K, Hayasaka K. Cardiac ion channel gene mutations in sudden infant death syndrome. *Pediatr Res*. 2008;64:482–487.
14. Tester DJ, McCormack J, Ackerman MJ. Prenatal molecular genetic diagnosis of congenital long QT syndrome by strategic genotyping. *Am J Cardiol*. 2004;93:788–791.
15. Cuneo BF, Ovadia M, Strasburger JF, Zhao H, Petropulos T, Schneider J, Wakai RT. Prenatal diagnosis and in utero treatment of torsades de pointes associated with congenital long QT syndrome. *Am J Cardiol*. 2003;91:1395–1398.
16. Hamada H, Horigome H, Asaka M, Shigemitsu S, Mitsui T, Kubo T, Kandori A, Tsukada K. Prenatal diagnosis of long QT syndrome using fetal magnetocardiography. *Prenat Diagn*. 1999;19:677–680.
17. Horigome H, Iwashita H, Yoshinaga M, Shimizu W. Magnetocardiographic demonstration of torsade de pointes in a fetus with congenital long QT syndrome. *J Cardiovasc Electrophysiol*. 2008;19:334–335.
18. Zareba W, Moss AJ, Schwartz PJ, Vincent GM, Robinson JL, Priori SG, Benhorin J, Locati EH, Towbin JA, Keating MT, Lehmann MH, Hall WJ. Influence of genotype on the clinical course of the long-QT syndrome: International Long-QT Syndrome Registry Research Group. *N Engl J Med*. 1998;339:960–965.
19. Beinder E, Grancay T, Menéndez T, Singer H, Hofbeck M. Fetal sinus bradycardia and the long QT syndrome. *Am J Obstet Gynecol*. 2001;185: 743–747.
20. Trippel DL, Parsons MK, Gillette PC. Infants with long-QT syndrome and 2:1 atrioventricular block. *Am Heart J*. 1995;130:1130–1134.
21. Moss AJ, Zareba W, Kaufman ES, Gartman E, Peterson DR, Benhorin J, Towbin JA, Keating MT, Priori SG, Schwartz PJ, Vincent GM, Robinson JL, Andrews ML, Feng C, Hall WJ, Medina A, Zhang L, Wang Z. Increased risk of arrhythmic events in long-QT syndrome with mutations in the pore region of the human ether-a-go-go-related gene potassium channel. *Circulation*. 2002;105:794–799.
22. Nagaoka I, Shimizu W, Itoh H, Yamamoto S, Sakaguchi T, Oka Y, Tsuji K, Ashihara T, Ito M, Yoshida H, Ohno S, Makiyama T, Miyamoto Y, Noda T, Kamakura S, Akao M, Horie M. Mutation site dependent variability of cardiac events in Japanese LQT2 form of congenital long-QT syndrome. *Circ J*. 2008;72:694–699.
23. Miura M, Yamagishi H, Morikawa Y, Matsuoka R. Congenital long QT syndrome and 2:1 atrioventricular block with a mutation of the SCN5A gene. *Pediatr Cardiol*. 2003;24:70–72.
24. Lupoglazoff JM, Cheav T, Baroudi G, Berthet M, Denjoy I, Cauchemez B, Extramiana F, Chahine M, Guicheney P. Homozygous SCN5A mutation in long-QT syndrome with functional two-to-one atrioventricular block. *Circ Res*. 2001;89:e16–e21.
25. Benson DW, Wang DW, Dyment M, Knilans TK, Fish FA, Strieper MJ, Rhodes TH, George AL Jr. Congenital sick sinus syndrome caused by recessive mutations in the cardiac sodium channel gene (SCN5A). *J Clin Invest*. 2003;112:1019–1028.
26. Hansen RS, Olesen SP, Grunnet M. Pharmacological activation of rapid delayed rectifier potassium current suppresses bradycardia-induced triggered activity in the isolated Guinea pig heart. *J Pharmacol Exp Ther*. 2007;321:996–1002.
27. Ten Harkel AD, Witsenburg M, de Jong PL, Jordaens L, Wijman M, Wilde AA. Efficacy of an implantable cardioverter-defibrillator in a neonate with LQT3 associated -arrhythmias. *Europace*. 2005;7:77–84.

CLINICAL PERSPECTIVE

The congenital long-QT syndrome (LQTS) diagnosed at perinatal life and through infancy is associated with high morbidity and mortality rates. However, data on the clinical presentation and genotype-phenotype correlation of this youngest age group of LQTS are limited. A nationwide survey was conducted in Japan, and 58 cases (18 fetuses, 31 neonates and 9 infants) were registered. Among them, the peak age at diagnosis was 0 to 2 days, and the 3 most frequent clinical presentations included sinus bradycardia, ventricular tachycardia/torsades de pointes, and atrioventricular block. The genotype was confirmed in 29 (71%) of 41 patients who underwent genotyping; the incidence resembled that of child LQTS. Patients who presented with early-onset ventricular tachycardia/torsades de pointes and atrioventricular block were almost exclusively those with LQT2 and LQT3 among the 3 major genes, but a considerable number of genetically unidentified ones were included. Sudden cardiac death/aborted cardiac arrest were prevalent in the latter. LQT1 patients tended to show only sinus bradycardia or positive family history of LQTS. These results mean that many life-threatening episodes observed in early-onset LQTS should be treated immediately and aggressively even without knowledge of the genotype. On the other hand, the present study was encouraging in that the outcome of patients was favorable with multiple pharmaceutical agents, typically with β-blockers, mexiletine, and magnesium and with pacemaker implantation/ implantable cardioverter-defibrillator, independent of the genotype. Further application of gene testing is needed to establish the most appropriate genotype-specific strategy for these patients.

Progress in Biophysics and Molecular Biology 110 (2012) 380–389

Contents lists available at SciVerse ScienceDirect

Progress in Biophysics and Molecular Biology

journal homepage: www.elsevier.com/locate/pbiomolbio

Review

Multi-scale simulations of cardiac electrophysiology and mechanics using the University of Tokyo heart simulator

Seiryo Sugiura*[,1], Takumi Washio[1], Asuka Hatano, Junichi Okada, Hiroshi Watanabe, Toshiaki Hisada

Department of Human and Engineered Environmental Studies, Graduate School of Frontier Sciences, The University of Tokyo, Kashiwanoha 5-1-5, Kashiwa-shi, Chiba 277-8563, Japan

ARTICLE INFO

Article history:
Available online 22 July 2012

Keywords:
Heart model
Computer simulation
Electrophysiology
Cooperativity
Fluid-structure interaction
Cardiac metabolism

ABSTRACT

The importance and need for an integrative mathematical modeling approach in the biological and medical fields is currently well recognized. Such an approach is crucial in understanding the complexity of hierarchical biological systems increasingly revealed by active researches in molecular and cellular biology. Particularly in cardiac functioning, modeling must cover such diverse phenomena as solid mechanics, fluid dynamics, electricity and biochemistry. Recent advancements in computational science and the development of high-performance computers have enabled the creation of multi-scale, multi-physics simulation heart models using the finite element method. Although whole heart or ventricular models of electrophysiology involving electro-mechanics with or without blood flow dynamics have been reported, to our knowledge no single model has yet succeeded in completely reproducing the behavior of the heart from the subcellular to whole organ levels. In this article, we present a brief methodology-focused review on some of the essential components for multi-scale, multi-physics heart modeling. A perspective of heart modeling in the era of high performance computing is also presented.

Contents

1. Introduction

Since the pioneering work of Noble (Noble, 1960), numerical simulation has been recognized as a powerful and indispensable tool for understanding the electrophysiology of the heart. Electrophysiology modeling is now applied to diverse cell types from many animal species in both normal and diseased conditions (Beeler and Reuter, 1977; Luo and Rudy, 1994; Stewart et al., 2009; Ten Tusscher et al., 2004; Ten Tusscher and Panfilov, 2006; Winslow et al., 2001). The explosion of knowledge obtained at the molecular level of ion channel activity necessitates the development of more detailed modeling (Silva et al., 2009). Several integrative approaches to coupling these cell models have been proposed, which have enabled cardiac electrical activity at the tissue or organ level to be reasonably well-simulated (Noble, 2002; Vigmond et al.,

* Corresponding author. Tel.: +81 3 58418393; fax: +81 3 58416376.
E-mail addresses: sugiura@k.u-tokyo.ac.jp (S. Sugiura), washio@sml.k.u-tokyo.ac.jp (T. Washio), asuka-h@sml.k.u-tokyo.ac.jp (A. Hatano), okada@sml.k.u-tokyo.ac.jp (J. Okada), nabe@sml.k.u-tokyo.ac.jp (H. Watanabe), hisada@mech.t.u-tokyo.ac.jp (T. Hisada).
[1] These authors equally contributed to this work.

0079-6107/$ – see front matter © 2012 Elsevier Ltd. All rights reserved.
http://dx.doi.org/10.1016/j.pbiomolbio.2012.07.001

2009). A similar history is found for the simulation of mechanical cardiac muscle activity, typically based on the cross-bridge model proposed by Huxley to describe skeletal muscle contraction (Huxley, 1957). In simulating the energy metabolism of heart muscle contraction, the cross-bridge model has been modified to account for the behavior of the cardiac myosins of distinct kinetic properties, and/or is coupled with ATP hydrolysis. Coupling of the cross-bridge model with the electrophysiology model via the inclusion of Ca^{2+} dependent regulatory mechanisms has enabled the excitation–contraction coupling process to be accurately simulated at the cellular level (Hunter et al., 1998; Landesberg and Sideman, 1994; Negroni and Lascano, 2008; Rice et al., 2008). From a clinical perspective, organ level simulation of the heart has significantly contributed to our understanding of hemodynamics (Beyar and Sideman, 1984; Sunagawa and Sagawa, 1982). Even so, earlier attempts to link these two levels failed to attract the broad-ranging interests of basic and clinical cardiology researchers.

Today, the importance and need for integrative approaches by mathematical modeling is well recognized in the biological and medical fields (Hunter and Borg, 2003). As emphasized by Hunter and Borg (2003), such needs stem from the complexity of hierarchical biological systems, which is being increasingly revealed by molecular and cellular biology studies. For example, imaging information on structure and function not only allow but force us to create a spatially distributed parameter model with realistic morphologies realized at levels from subcellular to whole organ. In the case of cardiac function, modeling must further embrace the diverse phenomena governed by the different physical principles involved, such as solid mechanics, fluid dynamics, electricity and biochemistry. Molecular simulation is expected to play a large role in future studies of this nature. Fortunately, recent advancements in computational science and the development of high-performance computers have enabled multi-scale, multi-physics simulation models of the heart to be constructed, using the finite element method (Lee et al., 2009; Noble, 2002; Trayanova, 2011). Whole heart or ventricular models of electrophysiology and electromechanics with or without flow dynamics in the chambers have been widely reported. However, to our knowledge, no single model has successfully reproduced the behavior of the heart at scales ranging from the subcellular to the whole organ.

In this article, we review and discuss some of the essential components and methodologies required for the development of a multi-scale, multi-physics heart simulation that integrates the molecular and cellular mechanisms of cardiac excitation, and contraction to reproduce the organ level electrophysiology and hemodynamics. Such a model could not only facilitate our understanding on how changes in molecular and cellular elements affect the macroscopic behavior of the heart, but may also supply detailed information on the micro-environment in which these elements are embedded in both physiological and pathological conditions.

In the concluding section, we present our own perspective on the potential use of super-computers for multi-scale simulation.

2. ECG simulation

A key aim of multiscale heart simulation is to establish the relation between the ion currents in the cell and the clinically obtained body surface ECG. Establishing this relationship is of paramount importance to clinical cardiology since it would improve clinical outcomes and pave the way for custom designed treatments. Because the basic framework for the development of the whole heart model of electrophysiology is well established, we here focus on reproducing the body surface potential map, or ECG, based on the cell model of electrophysiology. An alternative approach is to solve the inverse problem; however, due to the ill-posed nature of this problem, a reliable solution is currently available only for the cardiac surface (Ramanathan et al., 2004).

To obtain the body surface potential we need to solve the potential distribution in the model torso created by the electrical activity of the heart. Such simulations require huge computational resources, thus computational efficiency becomes a prime concern. Xue et al., assuming isotropic conductivity in the torso, coupled the bidomain model-based finite element method (FEM) to the boundary element method (BEM) in their study of T-wave morphology (Xue et al., 2009). In this approach, the FEM solution of the potential distribution in the anisotropic myocardium is first obtained. Using the potential on the heart boundary as the source term, the BEM problem is then solved to obtain the potential on the torso surface. This is an efficient way to solve the forward problem, but the advantage is lost if applied to torsos with numerous isotropic tissue types (Fischer et al., 2000). Furthermore, this is not a dynamic approach based on obtained source patterns independent of the torso.

The significant effect of different tissue conductivities on ECG morphology has also been noted (Keller et al., 2010). In our previous study, we also confirmed the effects of heterogeneity in torso conductivity (Washio et al., 2010). Taken together, realistic modeling of the torso allowing different tissue conductivities is a prerequisite of patient specific ECG simulation. In this context, an FEM model of the realistic torso has been applied to the simulation of body surface potential. However, most ECG simulations have, to date, adopted a two-step static approach consisting of the monodomain calculation of membrane potential of the heart domain and FEM solution of the torso following interpolation of membrane potential on the finite elements (Farina et al., 2009; Keller et al., 2011, 2010). Although the membrane potentials obtained by the monodomain model and the bidomain calculation do not appreciably differ (Potse et al., 2006), this finding may be undermined by further analysis. When applied to defibrillation, the bidomain model coupled to a realistic multi-tissue torso should definitely be subject to further analysis.

We have developed a parallel multilevel technique for the dynamic solution of the bidomain equation for heart electrophysiological analysis coupled with the torso (Washio et al., 2010). For the FEM solution of the discretized bidomain equations, we adopt a composite mesh composed of a fine (local) voxel mesh around the heart and a coarse (global) voxel mesh covering the torso because fine resolution is unnecessary for the extracellular domain outside the heart (Fig. 1). To conserve the electric currents in the local–global solution process, the Lagrangian multiplier method for the constraints at the interface of the local and global meshes is applied. A novel treatment to include the Purkinje fiber network in the local–global multi-grid algorithm is also introduced.

Using this technique, we simulated the human body surface ECG and analyzed the cellular basis of ECG wave form (Okada et al., 2011). The morphology of the human heart with a conduction system embedded in the torso model was based on computerized tomography (CT) scan data. Informed consent for the use of clinical data was granted by the Institutional Ethics Committee. In describing the electrophysiological properties, we adopted (for the appropriate elements) the ventricular myocyte model of Ten Tusscher and Panfilov (2006) and the Purkinje fiber model of Stewart et al. (2009). The network of the conduction system is modeled by one-dimensional elements and comprises a free-running (insulated) part connecting the atrioventricular node to the sites of earliest activation, and a network spreading from these sites along the endocardial surface. Network distribution was adjusted to reproduce the activation sequence of the human heart reported by Durrer et al. (1970). On the other hand, the distribution of different cell types, namely, endo-, M-, and epicardial cells, is

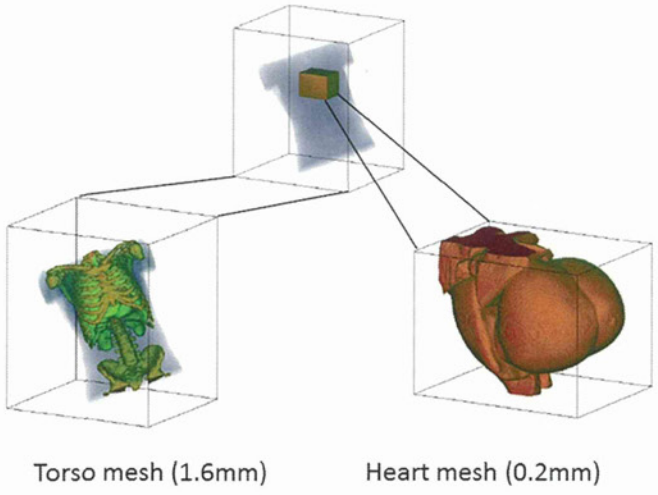

Fig. 1. Composite meshes for the multi-grid solver of the bidomain equation. The fine local voxel mesh (0.2 mm) domain around the heart and the global coarse voxel mesh (1.6 mm) domain covering the torso are used in model simulations.

unknown; thus we conducted an exhaustive search strategy for their most likely distribution in the ventricular wall. We varied the distribution of these cell types transmurally and also changed the action potential duration in the apico-basal direction in multiple combinations and simulated the electrical activity of heart and torso. An example of the time course of body surface potential during the QRS complex of the ECG is shown in Fig. 2. Comparing the body surface ECG obtained by various heart models with the body surface potential pattern, we concluded that both transmural and apico-basal gradients in repolarization (APD) contribute to the genesis of normal T-waves in human surface ECG (Fig. 3).

Estimating the cell distribution that best reproduces the ECG wave form in this manner constitutes a forward problem approach (as opposed to the inverse problem). Although about 6 h was required to calculate a single cardiac cycle in this study, with more advanced computation, the approach could be used to identify the most probable tissue properties which match a patients' individual ECG, and could thus become an invaluable tool in tailored medicine.

3. Sarcomere dynamics

As mentioned above, most of the contraction models used in heart simulation are based on the cycling cross-bridge model of Huxley (Huxley, 1957), in which myosin heads from the thick filament undergo a series of attachment–detachment cycles with the actin molecules of the thin filament. Incorporation of the Ca^{2+} dependent regulatory mechanism and/or compliant element into these models now allows accurate simulation of the experimental results obtained under a wide range of skeletal and cardiac muscle conditions, including the twitch contraction and force transient (Hunter et al., 1998; Landesberg and Sideman, 1994; Negroni and Lascano, 2008; Rice et al., 2008). However, to simulate heart activity, these models must capture the anomalously high Ca^{2+} sensitivity of activation over that of the skeletal muscle. The putative underlying basis of this sensitivity is co-operative interaction between sarcomere components. Among the postulated mechanisms are steric hindrance of tropomyosin by the strongly-bound cross-bridge, and the end-to-end interaction of troponin/tropomyosin units along the thin filament, both of which facilitate the formation of nearby cross-bridge, which then activates the strong response to Ca^{2+} ions. Obviously, the modeling of such mechanisms requires the description of spatially distributed states solved by either partial differential equations (PDE) or Monte Carlo (MC) simulations. The computational cost of these

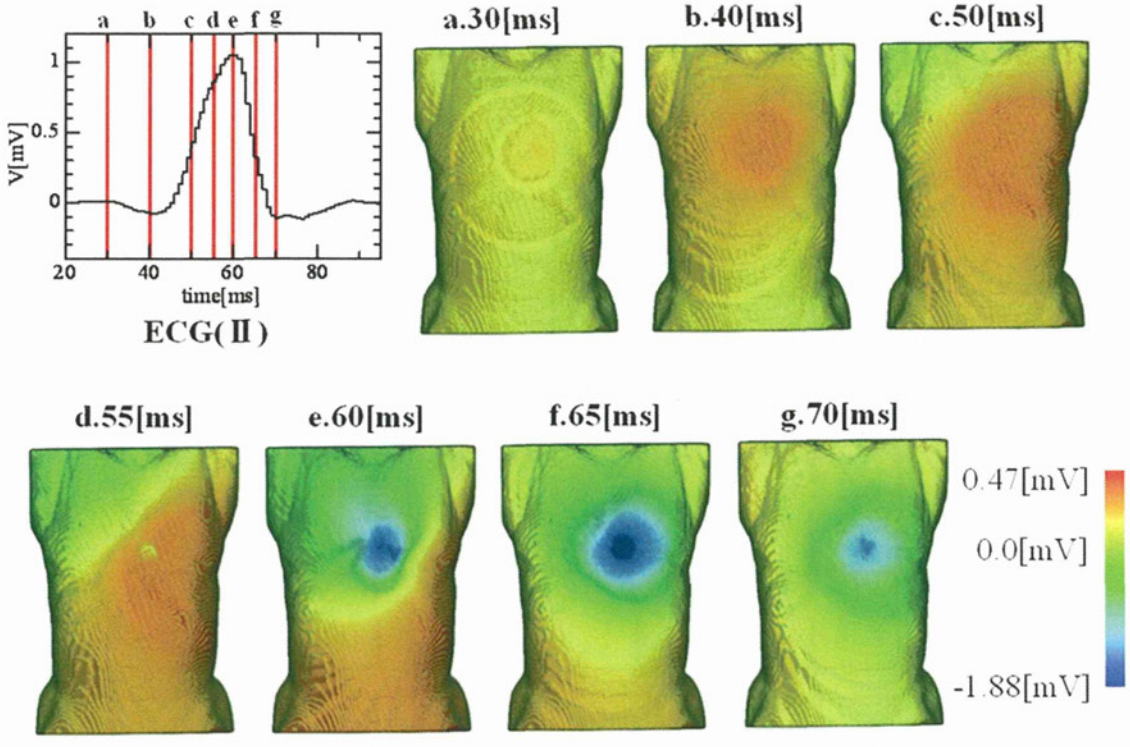

Fig. 2. Time lapse maps of the body surface potential during the activation phase. The timing of each map is indicated in the *top left* panel. *V*, voltage (from Fig. 2D of Okada et al. (Okada et al., 2011) with permission).

approaches has inspired the development of the mean field model, in which average behavior of the units is formulated by ordinary differential equations (ODEs) with phenomenological parameter tunings (Campbell, 1997; Hunter et al., 1998; Rice et al., 2008). Some of these approaches appear successful but are unable to reproduce the observed rapid force decay during twitch contractions.

Several spatially distributed models have been reported (Daniel et al., 1998; Hussan et al., 2006). In these models, the microanatomical arrangement of sarcomere is preserved and the transition rates of each functional unit are assumed to depend on the state of the neighboring unit and/or the cross-bridge strain. These models yield excellent agreement with experimental observation; however, as stated above, their numerical solution requires computationally expensive MC simulations, thus their application is limited to single sarcomeres or to myofilaments.

Two recent, unique approaches have circumvented the time consuming MC simulations. Rice et al. (2003) reported an analytical solution of their Ising model but the applicability of this approach seems to be limited to the steady state problem under a simple periodic boundary condition. Campbell et al. (2010) adopted a Markov model approach to formulate the transitions between states, which considered every possible combination of neighboring units, rendering their model applicable even to the dynamic twitch contraction. Again, however, the number of units in the model was too few to accurately model sarcomere because the number of required states in Markovian modeling grows explosively with the number of units.

We have developed a novel method for the numerical simulation of spatially-detailed sarcomere dynamics in which MC simulation results are approximated by an ODE (Washio et al., 2011). The framework of the model is schematically presented in Fig. 4. In the

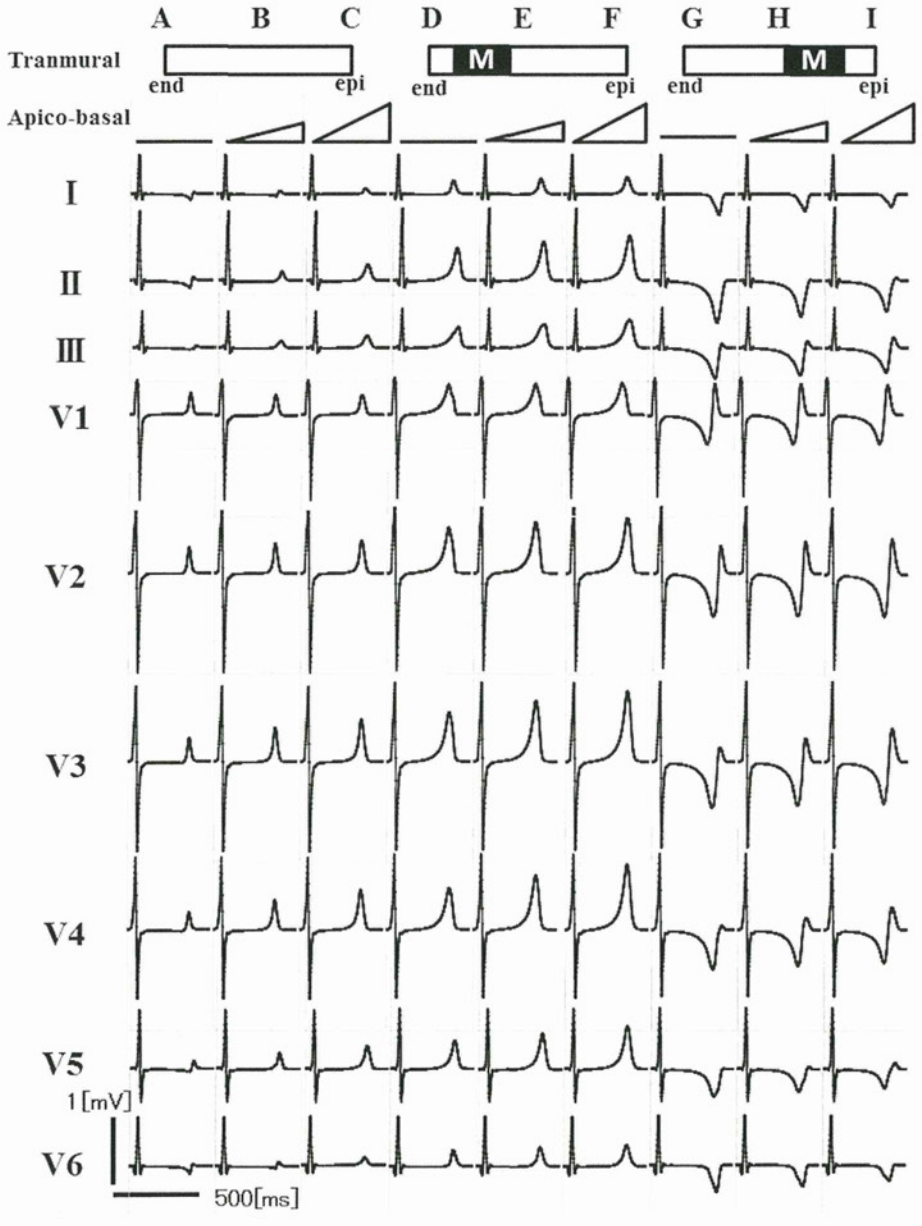

Fig. 3. Electrocardiogram obtained from nine combinations of the transmural and apicobasal APD gradients. *A*, *B*, and *C:* no transmural gradient and varying degree of apicobasal gradients. *D*, *E*, and *F:* M cells on the endocardial side and varying degree of apicobasal gradients. *G*, *H*, and *I:* M cells on the epicardial side and varying degree of apicobasal gradients (from Fig. 4 of Okada et al. (Okada et al., 2011) with permission).

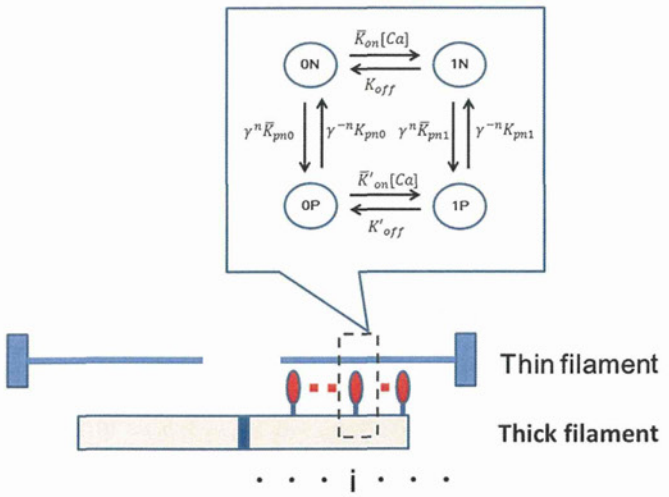

Fig. 4. Spatially-detailed model of sarcomere dynamics. Regulatory units assuming the complex of cross-bridge on the thick filament and regulatory proteins on the thin filament are arranged linearly. Each regulatory unit (indexed as "*i*") takes either of the 4 states defined by the combination of Ca^{2+} binding (1: bound, 0: not bound) and cross-bridge formation (P: permissive, N: non-permissive). Transition kinetics are adopted from Rice et al. (Rice et al., 2003). The rate constants of transition between the states ($\bar{K}_{on}, K_{off}, \bar{K}'_{on}, K'_{off}, K_{pn1}, \bar{K}_{pn1}, K_{pn0}, \bar{K}_{pn0}$) are modified by multiplication with either $[Ca^{2+}]$ or factors $\bar{\alpha}^n$ or $\bar{\alpha}^{-n}$ representing the states of the nearest neighbors.

model, 36 regulatory units representing the complex of cross-bridge and regulatory proteins are arranged linearly, mimicking the sarcomere structure. Each regulatory unit (indexed as "*i*") assumes either of the 4 states defined by the combination of Ca^{2+} binding (1: bound, 0: not bound) and cross-bridge formation (P: permissive, N: non-permissive). Transition kinetics are adopted from Rice et al. (2003), who assumed that transitions between the N and P states are governed by the states of their nearest neighbors, i.e., the transition rates are multiplied by the factor γ^n and γ^{-n}, where n is the number of P-state nearest-neighbors (inset of Fig. 4). Here, we define the vector representing the probability distribution of the ith unit as follows:

$$\mathrm{P}_i =^t \left[[0\mathrm{N}]_i, [1\mathrm{N}]_i, [1\mathrm{P}]_i, [0\mathrm{P}]_i\right]$$

$$\mathrm{P}_i^{\xi,\eta} =^t \left[[\xi, 0\mathrm{N}, \eta]_i, [\xi, 1\mathrm{N}, \eta]_i, [\xi, 1\mathrm{P}, \eta]_i, [\xi, 0\mathrm{P}, \eta]_i\right]$$

where ξ and η are the states of the neighboring unit of each side (N or P); thereby $[\xi, x, \eta]$ represents the combinatory probability of the ith unit being in state x (0N, 1N, 1P, or 0P) given that its respective neighbors are in states ξ and η.

The transition kinetics of the ith unit are described as follows:

$$\frac{dP_i}{dt} = \sum_{\xi,\eta=N,P} A_i(\xi,\eta)\cdot P_i^{\xi,\eta}$$

$$A_i(\xi,\eta) = \begin{bmatrix} -\bar{K}_{\mathrm{on}}[c\alpha] - \gamma^n\bar{K}_{np0} & K_{\mathrm{off}} & 0 & \gamma^{-n}K_{pn0} \\ \bar{K}_{\mathrm{on}}[c\alpha] & -K_{\mathrm{off}} - \gamma^n\bar{K}_{np1} & -\gamma^{-n}K_{pn1} & 0 \\ 0 & \gamma^n\bar{K}_{np1} & -\gamma^{-n}K_{pn1} - K'_{\mathrm{off}} & \bar{K}'_{\mathrm{on}}[C\alpha] \\ \gamma^n\bar{K}_{np0} & 0 & K'_{\mathrm{off}} & -\gamma^{-n}K_{pn0} - \bar{K}'_{\mathrm{on}}[c\alpha] \end{bmatrix}$$

Because this equation cannot be solved as an ODE without knowing the combinatory probabilities on the right hand side while the variables are the simple state probabilities, we estimated these values based on the MC simulation results.

Briefly, we performed MC simulation by applying dynamically changing Ca^{2+}-transients of various amplitudes. At each time step the number of combinatory states as well as the individual states was counted for each unit to yield the following matrix ($W_i(\xi,\eta)$)

$$P_i^{\xi,\eta} \approx W_i(\xi,\eta)\cdot P_i$$

$$W_i(\xi,\eta) = \begin{bmatrix} W_i(\xi,0\mathrm{N},\eta) & 0 & 0 & 0 \\ 0 & W_i(\xi,1\mathrm{N},\eta) & 0 & 0 \\ 0 & 0 & W_i(\xi,1\mathrm{P},\eta) & 0 \\ 0 & 0 & 0 & W_i(\xi,0\mathrm{P},\eta) \end{bmatrix},$$

which enables the problem to be solved as an ODE:

$$\frac{dP_i}{dt} = \sum_{\xi,\eta=N,P} A_i(\xi,\eta)\cdot W_i(\xi,\eta)\cdot P_i$$

The results obtained from this ODE agree favorably with the MC results (Fig. 5) The ODE simulation could also reproduce the experimental results under isometric and shortening twitch contractions (Washio et al., 2011). Moreover, the sarcomere dynamics of 1 s duration were solved in just 0.64 s using the ODE approximation, while the MC simulation required more than 1000 repeats to obtain reasonable mean values. Although it may be argued that this approach assumes the time-consuming MC simulation as the prerequisite, we have confirmed that the ***W*** matrix representing the Ca^{2+} transients can be applied to other independently obtained experimental transients to accurately model the force data. We consider that once the MC simulation has been conducted for a specific parameter set representing a given sarcomere property (itself driven mainly by properties of functional proteins) established under certain experimental conditions, e.g. pH or temperature, the ***W*** matrix can be used for any other simulations assuming the same cross-bridge property. Furthermore, if we prepare a set of ***W***'s and rate constants for various properties of proteins, for instance, myosins with different degrees of light chain phosphorylation (Davis et al., 2001), we can simulate the dynamics of the heart in which these different myosins are distributed throughout the ventricular wall.

Cooperativity is often defined and evaluated as the shape of the static force-pCa relationship, but it also significantly influences the force transient decay phase during the twitch contraction. In our previous study using the traditional ODE approach, physiological filling of the left ventricle, especially during the rapid filling phase, was not faithfully reproduced (Watanabe et al., 2004b). We will show how our new ODE model can solve this problem in the next section.

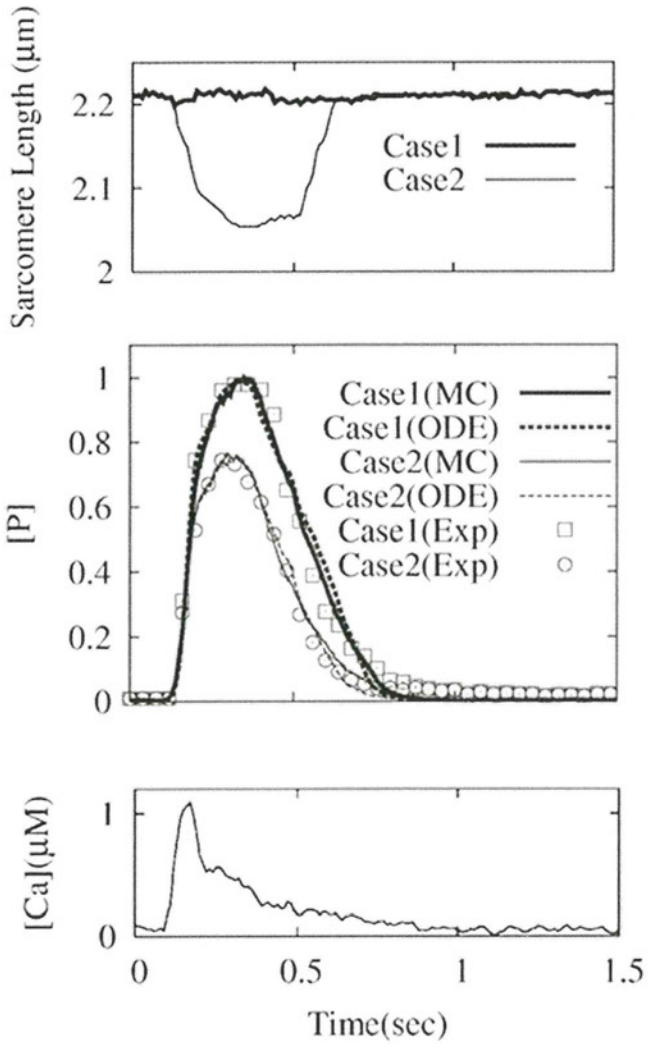

Fig. 5. Comparison between MC and ODE results. MC and ODE simulations were performed under isometric condition. Twitch forces ([*P*] values) in response to the two representative Ca^{2+} transients (top row) were calculated using MC (red circles) and ODE (solid lines) simulations at various sarcomere lengths (SL = 1.5, 1.8, 2.3 μm)(2nd to 4th rows).

4. Ventricular mechanics

The relation between the microscopic sarcomere model and the macroscopic ventricular mechanics was examined using the following finite element model of human ventricles. The model was based on our previous human heart model (Okada et al., 2011) and consisted of 77926 tetrahedral elements. We also created tetrahedral meshes in right and left ventricular cavities to calculate their volumes during the cardiac cycle. To each element of this heart model, we implemented the human ventricular myocyte model of electrophysiology (Ten Tusscher et al., 2004; Ten Tusscher and Panfilov, 2006) and our ODE model of sarcomere dynamics. We also modeled the fiber-sheet structure of myocardium by mapping fiber and sheet angles according to the literature (Costa et al., 1999). For the sheet angle distribution, their data sets (AF3) at base and apex were adopted and linearly interpolated to cover the whole ventricle.

The constitutive equation for passive myocardium was adopted from Usyk et al. with some modifications (Usyk et al., 2000):

$$W = \frac{C(e^Q - 1)}{2} + k_p(J-1)^2 + \xi I_1$$

$$Q = b_{ff}E_{ff}^2 + b_{ss}E_{ss}^2 + b_{nn}E_{nn}^2 + b_{fs}\left(E_{fs}^2 + E_{sf}^2\right) + b_{fn}\left(E_{fn}^2 + E_{nf}^2\right) + b_{ns}\left(E_{ns}^2 + E_{sn}^2\right)$$

where E_{ij} are components of Green's strain tensor defined in the local coordinate system having fiber, sheet and sheet-normal axes, J is the determinant of the deformation gradient tensor, and I_1 is the first principal reduced invariant. The second term in the first equation is volumetric energy term with $\kappa_p = 50$ kPa describing the nearly incompressible property and the third term was added to obtain the stability of the model with $\xi = 0.07$ kPa. Other material constants: $C = 0.88$ kPa; $b_{ff} = 5$; $b_{ss} = 6$; $b_{nn} = 3$; $b_{fs} = 10$; $b_{sn} = 2$; $b_{fs} = 2$ were adjusted to reproduce the physiologically relevant passive pressure-volume relation (Fig. 6B). Contraction was modeled by defining the uniaxial component (fiber direction) of active stress tensor as a function of active force calculated by the sarcomere model. The active stress tensor was added to the passive stress tensor calculated from above constitutive equations to yield the total stress.

For boundary conditions, we fixed the atrio-ventricular ring and coupled ventricular pressure to electrical analog of the circulation (Watanabe et al., 2004b). All the program codes were written in house and computation was performed using IBM Power 6 (JS22) with 128 cores.

Simulated pressure and volume during a single cardiac cycle are shown in Fig. 6A for left (LV: solid line) and right (RV: broken line) ventricles. Due to rapid decline of ventricular pressure attained by the co-operative activation of sarcomere, pressure waveforms became nearly rectangle rather than triangle in shape (upper panel). Time-volume curves (lower panel) can be clearly divided into four phases: 1) isovolumic relaxation phase (horizontal segments in the bottom), 2) early rapid filling phase, during which the majority of filling volume enters the ventricle, 3) diastasis (plateau phase of filling), 4) atrial contraction. All these features characterize the hemodynamics of normal human hearts (Leinihan et al., 1995; Little, 2001). Pressure–volume loops (Fig. 6B) also show normal cardiac function (LV Ejection fraction = 59%, RV ejection fraction = 50%) (Gentzler et al., 1974). In particular, the bottom part of the loop follows the exponential diastolic pressure-volume relation as reported in the literature for normal human hearts (Little, 2001). This physiological diastolic pressure–volume relation is an indication of complete relaxation and shows clear contrast to those reported in other electromechanical simulation studies (Gurev et al., 2010; Kerckhoffs et al., 2006). To further examine the effect of cooperativity on ventricular mechanics, we eliminated the cooperative effect from sarcomere model (setting $\gamma = 1$ in Fig. 4), and repeated the simulation. As shown in Fig. 6B, this intervention severely impaired both systolic and diastolic functions so that pressure–volume loops were compressed and shifted leftward (LV: red solid line, RV: red broken line). Because it was hard to gain insights from these distorted pressure–volume loops, we compared time–volume curves of LV with and without cooperativity by normalizing them relative to their maximum and minimum values (Fig. 6C). It is clearly seen that, without cooperativity (red line), early filling became slow and the fraction of filling volume during this period was decreased. These findings are considered as indications of diastolic dysfunction in clinical settings (Leinihan et al., 1995). On the other hand, ejection was accelerated by the elimination of cooperativity because cooperative mechanism of activation rather inhibits the force development at very low calcium concentration while enhancing it as concentration increases.

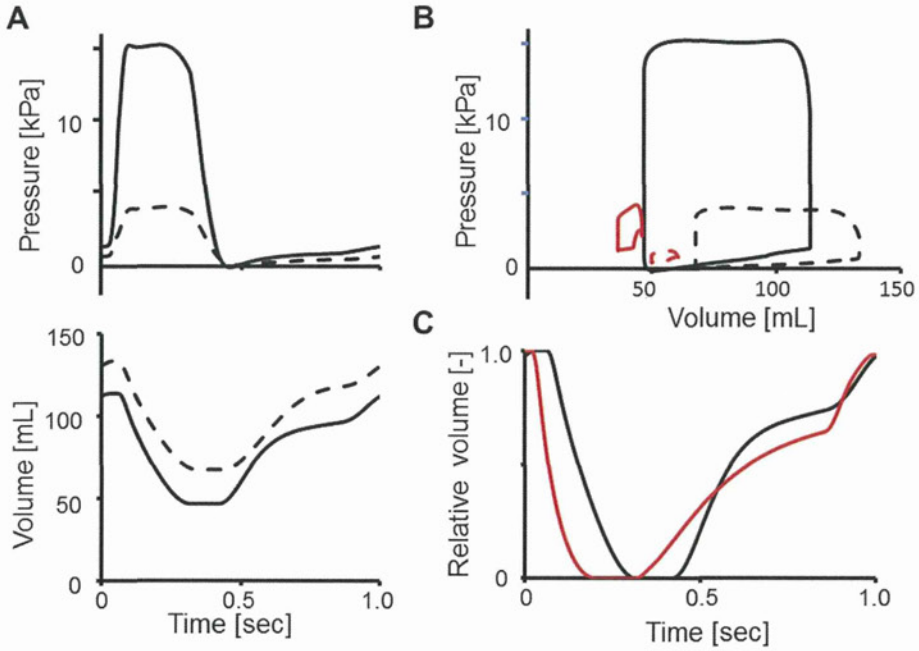

Fig. 6. Ventricular mechanics. A: Pressure (upper panel) and volume (lower panel) waveforms of left (solid line) and right (broken line) ventricles. B: Pressure-volume loops of left (solid line) and right (broken line) ventricles with (black) or without (red) cooperativity. C: Time-volume curves of the left ventricle normalized by its maximum and minimum values with (black) and without (red) cooperativity.

In addition to the sarcomere dynamics, many microscopic structural components are implicated in the ventricular mechanics. Among these, fiber orientation has been the focus of intensive studies and those studies unanimously reported a quasi-linear gradient of fiber angle across the ventricular wall (Ashikaga et al., 2004; Costa et al., 1999; Omens et al., 1991; Streeter et al., 1969). Simulation studies demonstrated that the optimal fiber distribution for homogeneous fiber strain during ejection (Rijcken et al., 1999) and for maximizing the external work is close to such anatomical measurements. Similarly, changes in laminar sheet angle during contraction have been reported (Ashikaga et al., 2005; Costa et al., 1999) and the simulation study has been attempted to find that incorporation of orthotropic model with sheet structure to the model yields better agreement with the measured strain distribution (Usyk et al., 2000). In this simulation, we also introduced the orthotropic passive property to reproduce the physiological diastolic pressure–volume relation, but further analyses are required to reveal the functional impact of sheet structure in more detail.

5. Hemodynamics

Because the essential function of the heart is to pump blood, fluid dynamics is an indispensable part of whole heart modeling and also an important issue in clinical cardiology. To date, however, only a few whole heart models have considered this aspect due to the complexity and the difficulty of the problem. To establish dynamic equilibrium, the kinematic energy of the blood flow is transferred from the contracting myocardial wall; such active contraction causes shape changes in the wall. In this sense, hemodynamics problems involve fluid structure interaction and large deformation analyses. The strategies adopted thus far include the immersed boundary method or moving boundary method (Kovacs et al., 2001; Nakamura et al., 2003) but the important clinical questions, such as the relation between the flow velocity distribution and the tissue property, remain unanswered. We have approached this problem using the Arbitrary Lagrangian Eulerian (ALE) finite element method with automatic mesh-updating developed in our laboratory (Zhang and Hisada, 2001), a form of interface-tracking. Briefly, the ALE forms of the Navier–Stokes equations are discretized in the fluid domain. On the structural domain, the equilibrium equations are formulated solely in Lagrangian form and discretized.

The fluid and structural domains are coupled by equating the displacement, velocity and acceleration on the interface through the element assemblage process. The system equations in the strong coupling method were solved simultaneously using a monolithic matrix.

Taking advantage of the computational accuracy and stability of this method, we have simulated the flow dynamics in the left ventricle during the cardiac cycle. In this simulation, pre- and after-loads to the left ventricle were modeled by the electric analog circuits of circulation with a contracting left atrium represented by the time-varying elastance (Alexander et al., 1987) (Fig. 7A). Propagation of excitation was formulated by the Fitz-Hugh-Nagumo model and the sarcomere dynamics were modeled by the 4-state Markov model. As observed in the human heart (Kilner et al., 2000), the inflow to the ventricle changes its direction to form a vortex and is finally squeezed out from the ventricle (Fig. 7B). As a result, only a fraction of the incoming blood during each diastole is ejected during the next systole. Our analysis revealed that blood entering during the first beat is completely cleared from the ventricle after around 9 beats at low heart rate (Watanabe et al., 2008). The functional significance of vortex formation is not clear but, at least in our analysis, the momentum of the blood heading towards the outflow tract was negligible and the kinetic energy of the ejected blood came principally from the work performed by the contraction of left ventricular myocardium. We have also found differences in the intra-ventricular flow patterns between the heart model with myocardial infarction and that of the normal heart during systole and diastole (Watanabe et al., 2004a). Furthermore, diastolic dysfunction (introduced by changing the parameter in the sarcoplasmic reticulum Ca^{2+} pump)

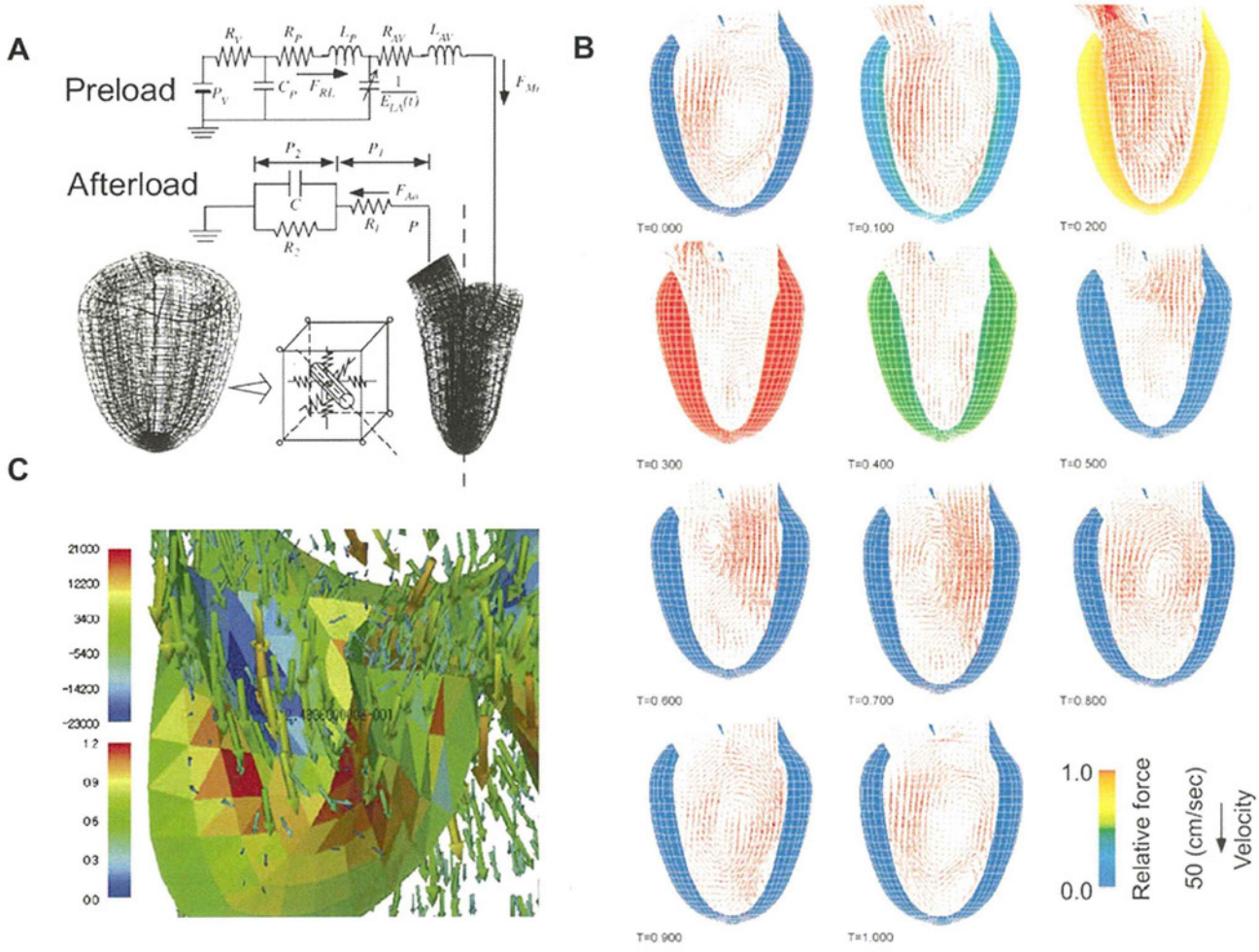

Fig. 7. Fluid structure interaction analysis of the left ventricular hemodynamics. **A:** Diagram of macroscopic model. FEM meshed for solid (ventricular wall) and fluid (blood) elements are shown with their electrical analogs of after load (systemic arterial tree) and preload (pulmonary circulation with active LA). PV, pulmonary source pressure; RV, source resistance; CP, pulmonary venous capacitance; RP, pulmonary resistance; LP, pulmonary inertance; RAV, atrioventricular resistance; LAV, atrioventricular inertance; FRL, pulmonary venous flow; FMi, blood flow through the mitral valve; qP and qLA, volumes of the pulmonary venous and LA. (From Fig. 2 of Watanabe et al. (Watanabe et al., 2004b) with permission). **B:** Time-lapse images of LV contraction and intraventricular blood flow. Numbers in each plate indicate the time following the onset of activation in seconds. Activation level (relative force) is shown in color coding. Velocity of blood is represented by the length of the arrows (from Fig. 4 of Watanabe et al. (Watanabe et al., 2004b) with permission). **C:** Stress in the leaflet and deformation of aortic valve. Close-up view of the leaflet in the late phase of ejection is shown with stress values in color coding (modified from Fig. 5A of Katayama et al. (Katayama et al., 2008) with permission).

impaired the diastolic rapid filling flow (unpublished data). These results highlight the importance of fluid-structure interaction analysis which could establish links between the subcellular molecular mechanics and the clinically observed hemodynamic parameters.

Another clinically important issue relevant to heart fluid dynamics is the motion of valves, which cause dramatic organ deformations in instances of high blood flow velocity. Previous aortic valve studies using either the commercially available software package (Nicosia et al., 2003) or the fictitious domain method (De Hart et al., 2003), were unable to analyze this problem at a physiologically relevant Reynolds number due to numerical instability. By employing the ALE finite element method with an automatic remeshing and reconnecting algorithm to correct for the large movement of the fluid-structure interface, we have been able to simulate the motion of aortic valve under a physiological Reynolds number ($\sim$3000, flow velocity $\fallingdotseq$ 1 m/s) (Katayama et al., 2008). In this analysis, anisotropic aortic valve leaflets were coupled to the short segment of the aorta. The sinus of Valsalva was found to facilitate the gradual but smooth closure of the valve by channeling blood into a vortex on the distal side of each leaflet during the early phase of ejection, thereby reducing stresses on the leaflet (Fig. 7C).

6. Conclusion and perspective

The need to integrate the vast amount of knowledge being gained at the molecular and cellular levels by comprehensive modeling is becoming more urgent, as understanding the function of the heart in depth will improve the accuracy and safety of clinical cardiology practices. The development and advancement of various novel diagnostic modalities requires that heart simulators be not only multi-scale but also multi-physics, in order to accurately compare with and examine multi-faceted clinical data. We have reviewed the necessary components and methodologies for the realization of such an electro-mechano-hemodynamic heart model. Assembly of these components to construct a comprehensive heart model is computationally costly but we have successfully developed a prototype model (Fig. 8 http://www.sml.k.u-tokyo.ac.jp/). With further validation and sophistication, and inclusion of missing components and details such as metabolism (Cortassa et al., 2006; Hatano et al., 2011), we hope

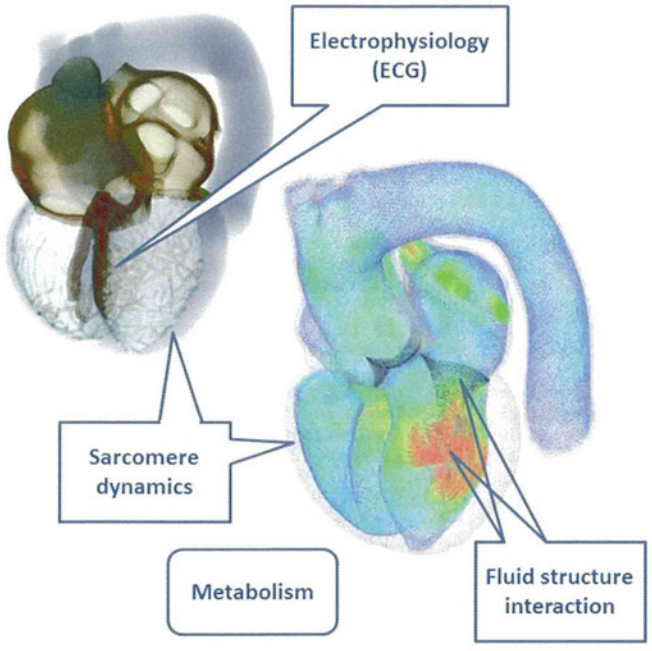

Fig. 8. Multi-scale, multi-physics heart simulation. The heart model on the left shows the propagation of excitation signals and the model on the right shows the blood flow in the heart chamber. The relevance of the indicated components is discussed in the text. Videos can be seen at http://www.sml.k.u-tokyo.ac.jp/.

that our heart simulator will become a valuable tool in clinical cardiology practice.

The starting point for the modeling process is an issue of ongoing debate (Noble, 2006). Due to present limitations in computational power, the cellular-level starting point of virtually all heart models is a lumped parameter system. Although apparently driven by the ionic current controlled by ion channels, pumps, or transporters, the functions of intracellular molecules are described in terms of per cell or per unit area of cell membrane, while ignoring their subcellular distributions (hence the term "lumped parameter model"). This "middle out" approach (Noble, 2006) has been successful to date and is also practical. However, if the starting point could be refined to a lower level to accommodate subcellular structure, the capability of the model to probe the mechanisms of intricate biological systems would be further intensified.

The capacity of high performance computers is increasing rapidly. In 2011, the K-computer developed by RIKEN and Fujitsu, comprising 864 computer racks equipped with a total of 88,128 CPUs, has achieved the world's highest LINPACK benchmark performance (10.51 petaflops). Even at this level of performance, a whole heart model based on the dynamics of each molecule in the myocyte could not be accomplished. However, the periodic nature of myocardial tissue may justify the computational technique of homogenization, by which a virtual heart composed of myocytes with subcellular structures, at least in part, may be maintained in the computer (Okada et al., 2010). Of course, this will be an enormous computational task with more than 10 trillion degrees of freedom, but we are aiming at its development.

Disclosure

The University of Tokyo/Graduate School of Frontier Sciences receives grant support from Fujitsu Ltd.

Editors' note

Please see also related communications in this issue by Constantino et al. (2012) and Takahashi and Naruse (2012).

Acknowledgment

This work was supported by the Japan Science and Technology Agency under grant Collaborative Development of Innovative Seeds-Practicability Verification Stage, and Japan Society for the Promotion of Science (JSPS) through its "Funding Program for World-Leading Innovative R&D on Science and Technology (FIRST Program)".

References

Alexander, J., Sunagawa, K., Chang, N., Sagawa, K., 1987. Instantaneous pressure-volume relation of the ejecting canine left atrium. Circ. Res. 61, 209–219.
Ashikaga, H., Covell, J.W., Omens, J.H., 2005. Diastolic dysfunction in volume-overload hypertrophy is associated with abnormal shearing of myolaminar sheets. Am. J. Physiol. 288, H2603–H2610.
Ashikaga, H., Criscione, J.C., Omens, J.H., Covell, J.W., Ingels, N.B., 2004. Transmural left ventricular mechanics underlying torsional recoil during relaxation. Am. J. Physiol. 286, H640–H647.
Beeler, G.W., Reuter, H., 1977. Reconstruction of the action potential of ventricular myocardial fibers. J. Physiol. 268, 177–210.
Beyar, R., Sideman, S., 1984. A computer study of the left ventricular performance based on fiber structure, sarcomere dynamics, and transmural electrical propagation velocity. Circ. Res. 55, 358–375.
Campbell, K., 1997. Rate constant of muscle force redevelopment reflects cooperative activation as well as cross-bridge kinetics. Biophys. J. 72, 254–262.
Campbell, S.G., Lionetti, F.V., Campbell, K.S., McCulloch, A.D., 2010. Coupling of adjacent tropomyosins enhances cross-bridge-mediated cooperative activation in a Markov model of the cardiac thin filament. Biophys. J. 98, 2254–2264.
Constantino, J., Hu, Y., Trayanova, N.A., 2012. A computational approach to understanding the cardiac electromechanical activation sequence in the normal and failing heart, with translation to the clinical practice of CRT. Prog. Biophys. Mol. Biol. 110 (2–3), 372–379.
Cortassa, S., Aon, M.A., O'Rourke, B., Jacques, R., Tseng, H.-J., Marban, E., Winslow, R.L., 2006. A computational model Integrating electrophysiology, contraction, and mitochondrial bioenergetics in the ventricular myocyte. Biophys. J. 91, 1564–1589.
Costa, K.D., Takayama, Y., McCulloch, A.D., Covell, J.W., 1999. Laminar fiber architecture and three-dimensional systolic mechanics in canine ventricular myocardium. Am. J. Physiol. 276, H595–H607.
Daniel, T.L., Trimble, A.C., Chase, P.B., 1998. Compliant realignment of binding sites in muscle: transient behavior and mechanical tuning. Biophys. J. 74, 1611–1621.
Davis, J.S., Hassanzadeh, S., Winitsky, S., Lin, H., Satorius, C., Vemuri, R., Aletras, A.H., Wen, H., Epstein, N.D., 2001. The overall pattern of cardiac contraction depends on a spatial gradient of myosin regulatory light chain phosphorylation. Cell. 107, 631–641.
De Hart, J., Peters, G.W., Schreurs, P.J., Baaijens, F.P., 2003. A three-dimensional computational analysis of fluid–structure interaction in the aortic valve. J. Biomech. 36, 103–112.
Durrer, D., van Dam, R.T., Freud, G.E., Janse, M.J., Meijler, F.L., Arzbaecher, R.C., 1970. Total excitation of the isolated human heart. Circulation 41, 899–912.
Farina, D., Jiang, Y., Dössel, O., 2009. Acceleration of FEM-based transfer matrix computation for forward and inverse problems of electrocardiography. Med. Biol. Eng. Comput. 47, 1229–1236.
Fischer, G., Tilg, B., Modre, R., Huiskamp, G.J.M., Fetzer, J., Rucker, W., Wach, P., 2000. A bidomain model based BEM-FEM coupling formulation for anisotropic cardiac tissue. Ann. Biomed. Eng. 28, 1229–1243.
Gentzler II, R.D., Briselli, M.F., Gault, J.H., 1974. Angiographic estimation of right ventricular volume in man. Circulation 50, 324–330.
Gurev, V., Constantino, J., Rice, J.J., Trayanova, N.A., 2010. Distribution of electromechanical delay in the heart: insights from a three-dimensional electomechanical model. Biophys. J. 99, 745–754.
Hatano, A., Okada, J., Washio, T., Hisada, T., Sugiura, S., 2011. A three-dimensional simulation model of cardiomyocyte integrating excitation-contraction coupling and metabolism. Biophys. J. 101, 2601–2610.
Hunter, P.J., Borg, T.K., 2003. Integration from proteins to organs: the Physiome Project. Nat. Rev. 4, 237–243.
Hunter, P.J., McCulloch, A.D., ter Keurs, H.E.D.J., 1998. Modeling the mechanical properties of cardiac muscle. Prog. Biophys. Mol. Biol. 69, 289–331.
Hussan, J., de Tombe, P.P., Rice, J.J., 2006. A spatially detailed myofilament model as a basis for large-scale biological simulations. IBM J. Res. Develop. 50, 583–600.
Huxley, A.F., 1957. Muscle structure and theories of contraction. Prog. Biophys. Biophys. Chem. 7, 255–318.
Katayama, S., Umetani, N., Sugiura, S., Hisada, T., 2008. The sinus of Valsalva relieves abnormal stress on aortic valve leaflets by facilitating smooth closure. J. Thorac. Cardiovasc. Surg. 136, 1529–1535.

Keller, D.U.J., Jarrousse, O., Fritz, T., Ley, S., Dossel, O., Seemann, G., 2011. Impact of physiological ventricular deformation on the morphology of the T-wave: a hybrid, static-dynamic approach. IEEE Trans. Biomed. Eng. 58, 2109–2119.

Keller, D.U.J., Weber, F.M., Seemann, G., Dossel, O., 2010. Ranking the influence of tissue conductivities on forward-calculated ECGs. IEEE Trans. Biomed. Eng. 57

Kerckhoffs, R.C.P., Neal, M.L., Gu, Q., Bassingthwaighte, J.B., Omens, J.H., McCulloch, A.D., 2006. Coupling of a 3D finite element model of cardiac ventricular mechanics to lumped systems models of the systemic and pulmonic circulation. Ann. Biomed. Eng. 35, 1–18.

Kilner, P.J., Yang, G.Z., Wilkes, A.J., Mohiaddin, R.H., Firmin, D.N., Yacoub, M.H., 2000. Asymmetric redirection of flow through the heart. Nature 404, 759–761.

Kovacs, S., McQueen, D.M., Peskin, C.S., 2001. Modelling cardiac fluid dynamics and diastolic function. Phil. Trans. R. Soc. A 359, 1299–1314.

Landesberg, A., Sideman, S., 1994. Mechanical regulation of cardiac muscle by coupling calcium kinetics with cross-bridge cycling. Am. J. Physiol. 267, H779–H795.

Lee, J., Niederer, S., Nordsletten, D., Le Grice, I., Smaill, B., Kay, D., Smith, N., 2009. Coupling contraction, excitation, ventricular and coronary blood flow across scale and physics in the heart. Phil. Trans. R. Soc. A 367, 2311–2331.

Leinihan, D.J., Gerson, M.C., Hoit, B.D., Walsh, R.A., 1995. Mechanisms, diagnosis, and treatment of diastolic heart failure. Am. Heart J. 130, 153–166.

Little, W.C., 2001. Assessment of normal and abnormal cardiac function. In: Braunwald, E., Zipes, D.P., Libby, P. (Eds.), Heart Disease. W.B. Saunders, Philadelphia.

Luo, C., Rudy, Y., 1994. A dynamic model of the cardiac ventricular action potential - simulations of ionic currents and concentration changes. Circ. Res. 74, 1071–1097.

Nakamura, M., Wada, S., Mikami, T., Kitabatake, A., Karino, T., 2003. Computational study on the evolution of an intraventricular vortical flow during early diastole for the interpretation of color M-mode Doppler echocardiograms. Biomech. Model. Mechanobiol. 2, 59–72.

Negroni, J.A., Lascano, E.C., 2008. Simulation of steady state and transient cardiac muscle response experiments with a Huxley-based contraction model. J. Mol. Cell. Cardiol. 45, 300–312.

Nicosia, M.A., Cochran, R.P., Einstein, D.R., Rutland, C.J., Kunzelman, K.S., 2003. A coupled fluid–structure finite element model of the aortic valve root. J. Heart Valve Dis. 12, 781–789.

Noble, D., 1960. Cardiac action and pacemaker potentials based on the Hodgkin-Huxley equations. Nature 188, 495–497.

Noble, D., 2002. Modelling the heart: from genes to cells to the whole organ. Science 295, 1678–1682.

Noble, D., 2006. The Orchestra: Organs and Systems of the Body, the Music of Life. Oxford University Press, New York. 74–87.

Okada, J., Washio, T., Hisada, T., 2010. Study of efficient homogenization algorithms for nonlinear problems approximation of a homogenized tangent stiffness to reduce computational cost. Comput. Mech. 46, 247–258.

Okada, J., Washio, T., Maehara, A., Momomura, S., Sugiura, S., Hisada, T., 2011. Transmural and apicobasal gradients in repolarization contribute to T-wave genesis in human surface ECG. Am. J. Physiol. 301, H200–H208.

Omens, J.H., May, K.D., McCulloch, A.D., 1991. Transmural distribution of three-dimensional strain in the isolated arrested canine left ventricle. Am. J. Physiol. 261, H918–H928.

Potse, M., Dubé, B., Richer, J., Vinet, A., Gulrajani, R.M., 2006. A Comparison of monodomain and bidomain Reaction-Diffusion models for action potential propagation in the human heart. IEEE Trans. Biomed. Eng. 53, 2425–2435.

Ramanathan, C., Ghanem, R.N., Jia, P., Ryu, K., Rudy, Y., 2004. Noninvasive electrocardiographic imaging for cardiac electrophysiology and arrhythmia. Nat. Med. 10, 422–428.

Rice, J.J., Stolovitzky, G., Tu, Y., de Tombe, P.P., 2003. Ising model of cardiac thin filament activation with nearest-neighbor cooperative interactions. Biophys. J. 84, 897–909.

Rice, J.J., Wang, F., Bers, D.M., de Tombe, P.P., 2008. Approximate model of cooperative activation and crossbridge cycling in cardiac muscle using ordinary differential equations. Biophys. J. 95, 2368–2390.

Rijcken, J., Bovendeerd, P.H.M., Schoofs, A.J.G., van Campen, D.H., Arts, T., 1999. Optimization of cardiac fiber orientation for homogeneous fiber strain during ejection. Ann. Biomed. Eng. 27, 289–297.

Silva, J.R., Pan, H., Wu, D., Nekouzadeh, A., Decker, K.F., Cui, J., Baker, N.A., Sept, D., Rudy, Y., 2009. A multiscale model linking ion-channel molecular dynamics and electrostatics to the cardiac action potential. Proc. Natl. Acad. Sci. USA 106, 11102–11106.

Stewart, P., Aslanidi, O.V., Noble, D., Noble, P.J., Boyett, M.R., Zhang, H., 2009. Mathematical models of the electrical action potential of Purkinje fibre cells. Phil. Trans. R. Soc. A 367, 2225–2255.

Streeter Jr., D.D., Spotnitz, H.M., Patel, D.P., Ross Jr., J.R., Sonnenblick, E.D., 1969. Fiber orientation in the canine left ventricle during diastole and systole. Circ. Res. 24, 339–347.

Sunagawa, K., Sagawa, K., 1982. Models of ventricular contraction based on time-varying elastance. Crit. Rev. Biomed. Eng. 7, 193–228.

Takahashi, K., Naruse, K., 2012. Stretch-activated BK channel and heart function. Prog. Biophys. Mol. Biol. 110 (2–3), 239–244.

Ten Tusscher, K.H.W.J., Noble, D., Noble, P.J., Panfilov, A.V., 2004. A model for human ventricular tissue. Am. J. Physiol. 286, H1573–H1589.

Ten Tusscher, K.H.W.J., Panfilov, A.V., 2006. Alternans and spiral breakup in a human ventricular tissue model. Am. J. Physiol. 291, H1088–H1100.

Trayanova, N.A., 2011. Whole-heart modeling Applications to cardiac electrophysiology and electromechanics. Circ. Res. 108, 113–128.

Usyk, T.P., Mazhari, R., McCulloch, A.D., 2000. Effect of laminar orthotropic myofiber architecture of regional stress strain in the canine left ventricle. J. Elasticity 61, 143–164.

Vigmond, E., Vadakkumpadan, F., Gurev, V., Arevalo, H., Deo, M.G.P., Trayanova, N., 2009. Towards predictive modelling of the electrophysiology of the heart. Exp. Physiol. 94, 563–577.

Washio, T., Okada, J., Hisada, T., 2010. A parallel multilevel technique for solving the bidomain equation on a human heart with Purkinje fibers and a torso model. SIAM Rev. 52, 717–743.

Washio, T., Okada, J., Sugiura, S., Hisada, T., 2011. Approximation for cooperative interactions of a spatially-detailed cardiac sarcomere model. Cell. Mol. Bioeng.

Watanabe, H., Sugano, T., Sugiura, S., Hisada, T., 2004a. Finite element analysis of ventricular wall motion and intra-ventricular blood flow in heart with myocardial infarction. JSME Internat. J. C. 47, 1019–1026.

Watanabe, H., Sugiura, S., Kafuku, H., Hisada, T., 2004b. Multiphysics simulation of left ventricular filling dynamics using fluid-structure interaction finite element method. Biophys. J. 87, 2074–2085.

Watanabe, H., Sugiura, S., Hisada, T., 2008. The looped heart does not save energy by maintaining the momentum of blood flowing in the ventricle. Am. J. Physiol. 294, H2191–H2196.

Winslow, R.L., Greenstein, J.L., Tomaselli, G.F., O'Rouke, B., 2001. Computational models of the failing myocyte: relating altered gene expression to cellular function. Phil. Trans. R. Soc. A 359, 1187–1200.

Xue, J., Gao, W., Chen, Y., Han, X., 2009. Identidy drug-induced T wave morphology changes by a cell-to-electrocardiogram model and validation with clinical trial data. J. Electrocardiol. 42, 534–542.

Zhang, Q., Hisada, T., 2001. Analysis of fluid-structure interaction problem with structural buckling and large domain change by ALE finite element method. Comput. Methods Appl. Mech. Engrg. 190, 6341–6357.

J Artif Organs (2012) 15:49–56
DOI 10.1007/s10047-011-0609-1

ORIGINAL ARTICLE

Engineering analysis of the effects of bulging sinuses in a newly designed pediatric pulmonary heart valve on hemodynamic function

Ichiro Suzuki · Yasuyuki Shiraishi · Shota Yabe · Yusuke Tsuboko · Telma Keiko Sugai · Ken Matsue · Takeyoshi Kameyama · Yoshifumi Saijo · Takashi Tanaka · Yoshihiro Okamoto · Zhonggang Feng · Takako Miyazaki · Masaaki Yamagishi · Makoto Yoshizawa · Mitsuo Umezu · Tomoyuki Yambe

Received: 7 February 2011 / Accepted: 6 September 2011 / Published online: 29 September 2011

Abstract The purpose of this study was to examine the hemodynamic characteristics of expanded polytetrafluoroethylene (ePTFE) pulmonary valves with bulging sinuses quantitatively in a pediatric pulmonary mechanical circulatory system designed by us, in order to propose the optimal design for clinical applications. In this study, we developed a pediatric pulmonary mock circulation system, which consisted of a pneumatic right ventricular model, a pulmonary heart valve chamber, and a pulmonary elastic compliance tubing with resistive units. The hemodynamic characteristics of four different types of ePTFE valves and a monoleaflet mechanical heart valve were examined. Relationships between the leaflet movements and fluid characteristics were evaluated based on engineering analyses using echocardiography and a high-speed video camera under the pediatric circulatory conditions of the mock system. We successfully performed hemodynamic simulations in our pediatric pulmonary circulatory system that could be useful for quantitatively evaluating the pediatric heart valves. In the simulation study, the ePTFE valve with bulging sinuses exhibited a large eddy in the vicinity of the leaflets, whereas the straight tubing exhibited turbulent flow. The Reynolds number obtained in the valve with bulging sinuses was calculated to be 1667, which was smaller than that in the straight tubing ($R_e = 2454$).

The hemodynamic characteristics of ePTFE pediatric pulmonary heart valves were examined in our mock circulatory system. The presence of the bulging sinuses in the pulmonary heart valve decreased the hydrodynamic energy loss and increased the systolic opening area. Based on an in vitro experiment, we were able to propose an optimal selection of pulmonary valve design parameters that could yield a more sophisticated pediatric ePTFE valve shape.

Keywords Pediatric pulmonary heart valve · ePTFE · Hemodynamic examination · Bulging sinus

I. Suzuki (✉) · S. Yabe · Y. Tsuboko · T. K. Sugai · Y. Saijo · M. Yoshizawa
Graduate School of Biomedical Engineering, Tohoku University, 4-1 Seiryo-machi, Aoba-ku, Sendai, Miyagi, Japan
e-mail: ichiro-rifle@pop02.odn.ne.jp

Y. Shiraishi (✉) · K. Matsue · T. Kameyama · T. Yambe
Institute of Development, Aging and Cancer, Tohoku University, 4-1 Seiryo-machi, Aoba-ku, Sendai, Miyagi, Japan
e-mail: shiraishi@idac.tohoku.ac.jp

T. Tanaka · Y. Okamoto · M. Umezu
Waseda University TWIns, Tokyo, Japan

Z. Feng
Department of Bio-System Engineering, Yamagata University, Yonezewa, Japan

T. Miyazaki · M. Yamagishi
Department of Pediatric Cardiovascular Surgery, Kyoto Prefectural University of Medicine, Kyoto, Japan

Introduction

Congenital cardiac malformations, such as tetralogy of Fallot and transposition of the great arteries, often result in right heart failure, which may require right ventricular outflow tract (RVOT) reconstruction. In these cases, it is necessary to reduce pulmonary arterial valve regurgitation [1–5].

The incidence of calcification in porcine bioprostheses and autologous pericardia is higher in children than in adults, which results in the poor durability of such valves in pediatric applications [6–14]. In order to reduce the generation of calcification, alternative materials such as ePTFE have been used in the fabrication of artificial valves.

Recently, the ePTFE valve with bulging sinuses shown in Fig. 1 has been applied to RVOT reconstruction. Yamagishi et al. [15, 16] reported RVOT reconstruction with the ePTFE valve with bulging sinuses in 325 patients from 2001 to 2011, none of whom had redo surgery due to valve malfunction related to calcification.

This excellent result motivated further attempts to improve the design and fabrication process of the ePTFE valves. However, there was a lack of information on the hemodynamic parameters associated with the mechanical structures involved in the design of the valve [17, 18]. The hypothesis of this study is that a vortex flow is generated in the vicinity of the bulging sinuses that results in optimal opening and closing of the leaflets. In this study, we developed a newly designed mechanical pulmonary circulatory system that facilitates the hemodynamic analysis of these artificial valves under the hydrodynamic conditions found in pediatric pulmonary circulation, and evaluated the hydrodynamic effects of the bulging sinuses on valve function.

Materials and methods

Valves employed

The valves examined in this study were as follows:

1. Monoleaflet mechanical heart valve (Björk–Shiley Monostrut)
2. Trileaflet ePTFE valve with bulging sinuses

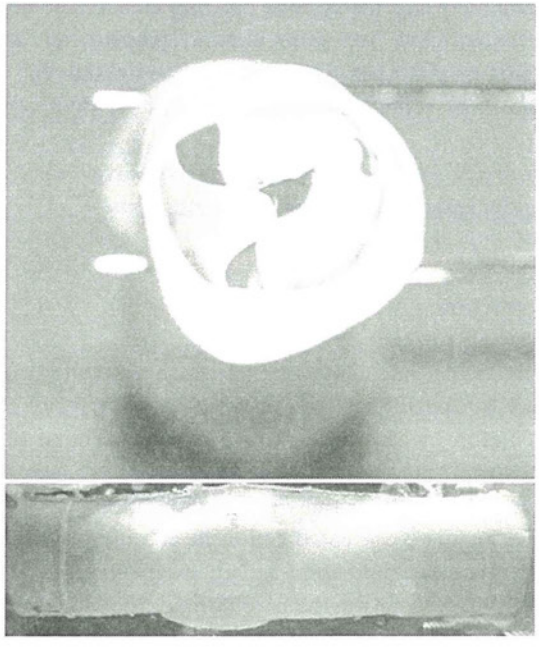

Fig. 1 Frontal and lateral views of an ePTFE valve with a bulging sinus

3. Trileaflet ePTFE valve in straight tubing without bulging sinuses

We employed a Björk–Shiley Monostrut valve for the mechanical settings of the mock circulatory system.

In the ePTFE valves, the conduit diameter and the thickness were 18 and 0.1 mm, respectively. To construct the bulging sinuses, an ePTFE sheet (thickness of 0.6 mm) was heated over a negative pressure in a vacuum pump, forcing it to fit to a mold of dome-shaped bulging sinuses. The cusps and these bulging sinuses were sutured along the conduit wall. In the conduits without bulging sinuses, the leaflets were sutured to the wall in the same area. There were two leaflet variations: fan-shaped and unfan-shaped.

The valved conduit with fan-shaped leaflets was fabricated with straight suture lines (S1) and curved bottom suture lines (S2), as shown in Fig. 2. The conduit with unfan-shaped leaflets was designed to allow a comparison of the effect of shape, and had straight suture lines (S1) and a point of suture (S3). A folded sheet was used to fabricate the valved conduit with unfan-shaped leaflets.

The two conduits were then compared.

We compared the effect of leaflet shape as well as the effect of bulging sinuses on the valvular characteristics. Figure 2 shows the four configurations analyzed in this study: (1) a valved conduit with bulging sinuses, B(+), and fan-shaped leaflets, F(+); (2) a straight valved conduit without bulging sinuses, B(−), and fan-shaped leaflets, F(+); (3) a valved conduit with bulging sinuses, B(+), and unfan-shaped leaflets, F(−); (4) a straight valved conduit without bulging sinuses, B(−), and unfan-shaped leaflets, F(−).

Pediatric pulmonary mock circulatory system

We developed a newly designed pediatric mechanical pulmonary circulatory system for the evaluation of valve function, as shown in Figs. 3 and 4. The system consisted of a right ventricular model, a valve chamber, an observation window, a reservoir tank, and a pulmonary arterial model with resistive units. The right ventricular model consisted of a cone-shaped silicone sac. The inflow portion of the right ventricular model was connected to the elastic right atrial rubber tubing. The valve to be evaluated was mounted in the valve chamber. The pulmonary arterial model was fabricated from silicone rubber. The resistance of the pulmonary arterial model was controlled by the resistive unit attached to the pulmonary arterial model.

Pulsatile flow was generated by a pneumatic artificial heart driver. Water at room temperature was used as the circulating medium. A bileaflet polymer valve was installed between the ventricle and the atrial model. These mechanical components were placed on the experimental table, and the mean inlet pressure of the ventricular model